上海交通大學

SHANGHAI JIAO TONG UNIVERSITY

学士学位论文

BACHELOR'S THESIS

论文题目： Van der Pol 模型的非平衡量子现象

学生姓名：	陈丹扬
学生学号：	517070910100
专　　业：	物理学 (国际班)
指导教师：	Carlos Navarrete-Benlloch
学 院 (系)：	物理与天文学院

上海交通大学
学位论文原创性声明

本人郑重声明：所呈交的学位论文《Van der Pol 模型的非平衡量子现象》，是本人在导师的指导下，独立进行研究工作所取得的成果。除文中已经注明引用的内容外，本论文不包含任何其他个人或集体已经发表或撰写过的作品成果。对本文的研究做出重要贡献的个人和集体，均已在文中以明确方式标明。本人完全意识到本声明的法律结果由本人承担。

学位论文作者签名：

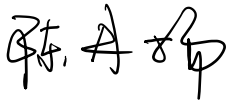

日期：2021 年 6 月 12 日

上海交通大学
学位论文版权使用授权书

本学位论文作者完全了解学校有关保留、使用学位论文的规定，同意学校保留并向国家有关部门或机构送交论文的复印件和电子版，允许论文被查阅和借阅。本人授权上海交通大学可以将本学位论文的全部或部分内容编入有关数据库进行检索，可以采用影印、缩印或扫描等复制手段保存和汇编本学位论文。

保密□，在___年解密后适用本授权书。

本学位论文属于

不保密☑。

（请在以上方框内打“√”）

学位论文作者签名：

日期：2021年6月12日

指导教师签名：

日期：2021年6月12日

Van der Pol 模型的非平衡量子现象

摘　要

Frank Wilczek 在 2012 年提出的时间晶体激起了物理学家们对在不同情况下打破时间平移对称性的强烈兴趣。利用现代平台，如超导电路，我们的论文提出了利用 Van der Pol 振子在开放系统中实现时间晶体结构的方案。经典条件下的 Van der Pol 振子在处于有限环相时，存在典型的周期性振荡行为，这是正我们在量子系统中所追求的。首先，我们提出了一种使用超导回路，基于下转换的搭建单个 Van der Pol 振子的方法。通过解析方法和数值研究我们证明了，量子涨落会导致单个 Van der Pol 振子在有限时间内达到平衡，最终停留在这个没有时间晶体结构的稳态。进一步，我们已知耦合的 Van der Pol 晶格具有同步效应，这直接启发了我们下一步的研究内容。我们定义相位的方差来表示系统对于时间晶体结构的维持程度，较小的方差表明系统仍然保持时间晶体状态。我们通过精确的数值模拟和近似的解析方法表明，对于一维、二维、三维和全耦合晶格，耦合效应抑制了方差增长。我们还注意到，在耦合生效之前，所有这些系统都经历了一个初始方差增长阶段。对于耦合连通性有限的系统（1D、2D 和 3D），这种初始方差偏移与系统规模的正幂成正比。对于宏观系统，这会最终消除他们的振荡行为。而数值模拟表示，全耦合系统具有一个与系统规模无关的方差偏移。因此我们证明了，在宏观的全耦合系统中，对量子涨落具有鲁棒性的自维持振荡存在。

关键词：非平衡统计、线性化、时间晶体

NONEQUILIBRIUM QUANTUM PHENOMENA THROUGH THE VAN DER POL MODEL

ABSTRACT

Frank Wilczek's proposal of the time crystal in 2012 has been giving physicists strong inspirations to break time-translation symmetry under different circumstances. Taking advantage of modern platforms such as superconducting circuits, our thesis propose an architecture making use of Van der Pol oscillators to achieve time-crystalline order in an open system. Classically, Van der Pol oscillators have oscillatory behaviors in a limit-cycle phase, which is what we pursuit quantum mechanically. First, making use of the down-conversion process implementable on superconducting circuits, we present a method to build a Van der Pol oscillator with superconducting circuits. According to both analytical and numerical study, we show that in finite time the quantum fluctuation lead a single Van der Pol oscillator to equilibrium, which is a steady state without time-crystalline order. Further on, it's known that coupled Van der Pol lattice have synchronization effect, which inspires our next investigation. We define phase variance to represent the maintenance of time-crystalline order, which is kept when variance is small. We show by exact numerical simulations and approximate analytical methods that, for 1D, 2D, 3D and all-to-all coupled lattices, the variance growth is suppressed by the coupling effect. However, we also observe that all these systems experience an initial variance growth stage before coupling come into effect. For systems with finite coupling connectivity (1D, 2D and 3D), such initial variance grows to a value proportional to a positive power of system's size. For macroscopical systems, it will kill the oscillatory behavior eventually. In contrast, simulation shows all-to-all coupled system has a constant variance bias, independent from the system size. Hence we prove the existence of spontaneous self-sustained oscillations that are robust against quantum fluctuations, in a macroscopical all-to-all coupled system.

Key words: Nonequilibrium statistics, Linearization, Time crystal

Contents

Chapter 1 Introduction

Modern platforms such as superconducting circuits allow us to implement many-body models that include driving and dissipation. Nowadays, with quantum optical techniques, it is possible for physicists to precisely control each mode in the many-body model. It will enable us to reach phases of matter that are difficult to reach in real materials and explore new physics. In this thesis, we focus on the time-crystalline order and manage to construct such elusive phase of matter with coupled Van der Pol lattices.

Wilczek proposed the concept of time crystal in 2012[1-2], which is a system self-organizing in time that breaks time-translational symmetry spontaneously. However, Watanabe et al. proved the absence of time-crystals in a closed system[3], dominated by a Hamiltonian. Fortunately, this no-go theorem is proven under very restrictive conditions, and inspired by Wilczek's original ideas, researchers have explored different possible ways out. The simplest one is when the Hamiltonian has a constant of motion, such that, even at equilibrium, the system might be forced to oscillate in order to satisfy the corresponding constraint (this is what happens with superfluid time crystals, which oscillate at a frequency proportional to the chemical potential[4]). Another popular way out[5] has consisted on driving periodically the system, such that now it is only invariant under discrete time-translational invariance, a symmetry that can indeed be spontaneously broken. Finally, coming back to continuous time-translational symmetry breaking, people have also studied the possibility of using open systems[6], which being out of equilibrium, do not need to satisfy the no-go theorem. So far, however, there is no completely satisfactory open model leading to robust time-crystalline order in the quantum regime. It is in this last context where our study takes place.

The basic model we apply is the quantum Van der Pol oscillator, a simple particle-non-conservative system with incoherent pumping and non-linear damping. Classically, the Van der Pol system[7] evolve in limit cycles in certain condition, which results in deterministic chaos[8]. Lee et al.[9] introduced a method to construct a quantum Van der Pol oscillator with trapped ions. In such a quantum system, the fluctuations destroy the classical limit cycles, and the system reaches a steady state[10]. When coupled together, both classical and quantum Van der Pol oscillators in this phase display synchronization and phase lock phenomena effect[9, 11-12]. Most works study all-to-all coupled lattices[13-14], and showing the synchronization phase transition with mean field method and considering only classical fluctuations.

In this thesis, we first propose an architecture to implement a quantum Van der Pol oscillator, as well as a coupled Van der Pol lattice, by exploiting the down-conversion process available in superconducting circuits[15]. We study under which circumstances this system maintains a state that has time-crystalline behavior, that is, oscillatory behavior, which should be robust against quantum fluctuations. According to both analytical and numerical study, we show that, in finite time, the quantum noise lead a single Van der Pol oscillator to losing time-crystalline order. It will only be achieved in the classical limit, with infinite number of excitations, which is impossible in any physical systems.

Based on the idea that coupled Van der Pol model displays phase-lock phenomena, we then analyze the coupled Van der Pol lattices for their ability to resist quantum fluctuations in the non-equilibrium processes. With exact numerical simulations for 1D, 2D, 3D and all-to-all coupled lattice and approximate analytical methods for 1D, we show that after a certain time, all of the coupled systems are capable of reaching a phase where the effect of quantum fluctuations is halted. We find the variance, which determines the time-crystalline order if kept small, is suppressed by a factor proportional to the lattice size. For a macroscopical lattice, the quantum fluctuations are frozen by coupling effect. However, we also find that the system experiences an initial variance growth. For 1D, 2D and 3D lattices, such initial variance end up scaling with a positive power of the lattice size, which means that by the time the quantum fluctuations are suppressed, the time-crystalline order is already lost. This is not the case for the all-to-all coupled model, whose initial variance is a constant independent of the system size. As a result, time crystalline order is achieved in a finite time for a large all-to-all coupled system.

Chapter 2 Preliminaries and background

2.1 Open quantum systems

A closed quantum system can be fully described by a Hamiltonian $\hat{H}$, with Schrödinger equation $i\hbar\partial_t\hat{\rho} = \left[\hat{H}, \hat{\rho}\right]$. However, in the real world, systems are rarely closed, but open. These systems interact with other ones, which experimentalists do not have access to, generally dubbed, 'environment'. In our thesis, the Van der Pol system is an open system with non-linear dissipation.

We will now introduce one of the description of the open quantum systems, master equations. Here is an example of a simplest quantum system. Consider a closed system consisted of a cavity mode $\hat{a}$ and an external field, described by a continuous set $\hat{b}(\omega)$, interacting. These annihilation operators satisfy canonical commutation relationships $\left[\hat{a}, \hat{a}^\dagger\right] = 1$ and $\left[\hat{b}(\omega), \hat{b}^\dagger(\omega')\right] = \delta(\omega - \omega')$. Any other combination of operators commute. Tracing the external mode off later, the cavity mode a can be regarded as a typical open system. Before doing that, we first focus on the composite system, described by a Hamiltonian $\hat{H} = \hat{H}_{cav} + \hat{H}_{ext} + \hat{H}_{int}$, where

$$\begin{aligned}
\hat{H}_{cav} &= \hbar\omega_c \hat{a}^\dagger \hat{a}, \\
\hat{H}_{ext} &= \int_0^\infty d\omega \hbar\omega \hat{b}^\dagger(\omega)\hat{b}(\omega), \\
\hat{H}_{int} &= i\hbar\sqrt{\frac{\gamma}{\pi}} \int_0^\infty d\omega \left[\hat{b}(\omega)^\dagger \hat{a} - \hat{b}(\omega)\hat{a}^\dagger\right].
\end{aligned} \tag{2–1}$$

$\sqrt{\gamma/\pi}$ is a coupling constant. This interaction Hamiltonian is written under several assumptions: there are no non-linear optical effects; the contribution from the coupling medium (for example, a half-transmitted mirror) to the Hamiltonian is quadratic in annihilation and creation operators; the interaction is perturbative; and finally, the mirror's transmissivity is independent of ω.

Now we assume the external state $\hat{\rho}_{ext}$ is a displaced thermal state, which is general enough for an environment. It has the displacement $\alpha(\omega)$, and thermal photon number $\bar{n}$.

First, we move the external field to a displaced picture, and it will take the external field to a thermal state. Also, the initial Hamiltonian gets a new term $\hat{H}_{inj}$, representing the displacement, or laser driving:

$$\begin{aligned}
&\hat{H}_D = \hat{H}_{cav} + \hat{H}_{ext} + \hat{H}_{int} + \hat{H}_{inj}, \\
&\text{where } \hat{H}_{inj} = i\hbar\left[\mathcal{A}(t)\hat{a}^\dagger - \mathcal{A}^*(t)\hat{a}\right] \\
&\text{and } \mathcal{A} = -\sqrt{\gamma/\pi}\int_{-\infty}^{\infty} d\omega e^{i\omega t}\alpha(\omega).
\end{aligned} \tag{2–2}$$

Using $\hat{U}_c = e^{-i\omega_c\hat{a}^\dagger\hat{a} + \mathcal{B}(t)\hat{a}^\dagger - \mathcal{B}^*(t)\hat{a}} e^{-i\int_{-\infty}^{\infty} d\omega\omega\hat{b}^\dagger(\omega)\hat{b}(\omega)}$, we move to the interaction picture, and here $\mathcal{B}(t) = \int_0^t dt'\mathcal{A}(t')$. Now we have removed all rotation and displacement into the operators: $\hat{\rho}_I = \hat{U}_c^\dagger\hat{\rho}\hat{U}_c$ and $\hat{a}_I = \hat{U}_c^\dagger\hat{a}\hat{U}_c$. Our Hamiltonian becomes:

$$\hat{H}_I(t) = i\hbar\sqrt{\frac{\gamma}{\pi}}\int_{-\infty}^{+\infty} d\omega\left[e^{i\omega t}\hat{b}^\dagger(\omega)\hat{a}_I(t) - e^{-i\omega t}\hat{b}(\omega)\hat{a}_I^\dagger(t)\right] \tag{2–3}$$

To simplify equation (2–3), the theory makes these approximations: $\hat{\rho}_I(t)$ is always close to $\hat{\rho}_{cav,I}(t) \otimes \hat{\rho}_{ext,I}(t)$ in first order; there is no back reaction; it can be approximated in second order. Finally, after tracing out $\hat{b}$ and move back to the Schrödinger picture, we arrive a general result for an open system:

$$\begin{aligned} &\partial_t \hat{\rho}_{cav} = \frac{1}{i\hbar}\left[\hat{H}_S, \hat{\rho}_{cav}\right] + (\bar{n}+1)\gamma \mathcal{D}_{\hat{a}}[\hat{\rho}_{cav}] + \bar{n}\gamma \mathcal{D}_{\hat{a}^\dagger}[\hat{\rho}_{cav}], \\ &\text{where } \hat{H}_S = \hat{H}_{cav} + \hat{H}_{inj}, \\ &\text{and } \mathcal{D}_{\hat{J}}[\hat{\rho}_0] = 2\hat{J}\hat{\rho}_0\hat{J}^\dagger - \hat{J}^\dagger\hat{J}\hat{\rho}_0 - \hat{\rho}_0\hat{J}^\dagger\hat{J}. \end{aligned} \tag{2–4}$$

Remind $\bar{n}$ is the expectation of $\hat{b}^\dagger\hat{b}$ of the external state. This equation is know as the master equation with two kinds of terms. The first one is the familiar Hamiltonian term, Hermitian. The other ones are superoperators, specifically called Lindbladian $\mathcal{D}_{\hat{J}}[\hat{\rho}]$, defining the non-Hermitian quantum jump. These terms combine into $\partial_t\hat{\rho} = \mathcal{L}[\hat{\rho}]$, where the generator of dynamics $\mathcal{L}$ is known as Liouville superoperators, or Liouvillian.

2.2 Effective theory: eliminating spurious degrees of freedom

When we studying practical models, we always use effective theory to eliminate some degrees of freedom and focus on a relevant system we need. There are theories for both closed systems and open ones, and now we will introduce the projection superoperators method for eliminate the irrelevant part from an open system. For simplicity, we call the relevant part "system" and the irrelevant part "environment". We can separate the total Hilbert space by defining $\mathcal{H} = \mathcal{H}_S \otimes \mathcal{H}_E$.

An open system can be described by a master equation as we mentioned in 2.1, and now we give a very general form of it:

$$\partial_t\hat{\rho} = \mathcal{L}[\hat{\rho}]. \tag{2–5}$$

The Liouvillian consists of all kinds of Hermitian terms and non-Hermitian terms. Then we divide it into two kinds: free Liouvillian $\mathcal{L}_0$ and interaction Liouvillian $\mathcal{L}_1$. $\mathcal{L}_0$ only contains the terms that do not connect system and environment, and vice versa. Free Liouvillian can be easily written with two parts: free system's and free environment's by $\mathcal{L}_0 = \mathcal{L}_S + \mathcal{L}_E$.

We need two projection superoperators to map from $\mathcal{H}$ to $\mathcal{H}_S$. They are defined in (2–6)

$$\mathcal{P} + \mathcal{Q} = 1,\ \mathcal{P}\mathcal{L}_0\mathcal{Q} = \mathcal{Q}\mathcal{L}_0\mathcal{P} = 0 \text{ and } \mathcal{P}\mathcal{L}_1\mathcal{P} = 0 \tag{2–6}$$

$\mathcal{P}$ has the property $\mathcal{P}[\hat{\rho}] = \mathrm{tr}_\mathrm{E}\{\hat{\rho}\} \otimes \bar{\rho}_\mathrm{E}$, where $\mathcal{L}_\mathrm{E}\left[\bar{\rho}_\mathrm{E}\right] = 0$. With second order approximation and $\mathcal{Q}[\hat{\rho}(0)] = 0$, a dynamic equation for $\mathcal{P}[\hat{\rho}]$ can be derived by integrating a dynamic equation for $\mathcal{P}[\hat{\rho}]$:

$$\partial_t\mathcal{P}[\hat{\rho}] \approx \mathcal{P}\mathcal{L}_0\mathcal{P}[\hat{\rho}] + \int_0^t d\tau \mathcal{P}\mathcal{L}_1 e^{\mathcal{L}_0\tau}\mathcal{L}_1\mathcal{P}[\hat{\rho}(t-\tau)] \tag{2–7}$$

Moreover, we assume that the interaction Liouvillian can be described by a Hamiltonian:

$$\mathcal{L}_1[\hat{Y}] = \left[\frac{\hat{H}_1}{\mathrm{i}\hbar}, \hat{Y}\right], \text{ where } \hat{H}_1/\hbar = \sum_{m=1}^{M} g_m \hat{S}_m \otimes \hat{E}_m \tag{2–8}$$

Mow the integration in Eq. (2–7) becomes

$$\sum_{m,n=1}^{M} g_m g_n \big(\hat{S}_n e^{C_{mn}(\tau)\mathcal{L}_S \tau} \left[\hat{\rho}_S(t-\tau)\hat{S}_m\right] - K_{nm}(\tau)\hat{S}_n e^{\mathcal{L}_S \tau}\left[\hat{S}_m \hat{\rho}_S(t-\tau)\right]\big) + \text{H.c.} \tag{2–9}$$

where C_{mn} and K_{nm} are two-time correlators using quantum regression theorem.

$$\begin{aligned} C_{mn}(\tau) &= \text{tr}_E\left\{\hat{E}_n e^{\mathcal{L}_E \tau}\left[\bar{\rho}_E \hat{E}_m\right]\right\} = \lim_{t\to\infty}\left\langle \hat{E}_m(t)\hat{E}_n(t+\tau)\right\rangle_E \\ K_{nm}(\tau) &= \text{tr}_E\left\{\hat{E}_n e^{\mathcal{L}_E \tau}\left[\hat{E}_m \bar{\rho}_E\right]\right\} = \lim_{t\to\infty}\left\langle \hat{E}_n(t+\tau)\hat{E}_m(t)\right\rangle_E \end{aligned} \tag{2–10}$$

Finally, we assume the correlators are either zero or a fast decay in time, then the system is mainly dominated by $\mathcal{L}_S$. If $\mathcal{L}_S[\hat{\rho}] = i\hbar\left[\hat{H}_S, \hat{\rho}\right]$, the effective time-local master equation can reads

$$\partial_t \hat{\rho}_S \approx \mathcal{L}_S\left[\hat{\rho}_S\right] + \sum_{m=1}^{M} g_m g_n \int_0^t d\tau \big[C_{mn}(\tau)\hat{S}_n \hat{\rho}_S(t)\tilde{S}_m(\tau) - K_{nm}(\tau)\hat{S}_n \tilde{S}_m(\tau)\hat{\rho}_S(t)\big] + \text{H.c.} \tag{2–11}$$

2.3 Phase space representations

In quantum mechanics, position and momentum don't commute, and their observables can't take definite values. What we can do is describing the probability distribution for X and P, or α in a complex plane.

2.3.1 Different phase-space representations

A general definition for such probability distribution is

$$\begin{aligned} F_\rho^z(\alpha) &= \int_{\mathbb{C}} \frac{1}{\pi} e^{\beta^*\alpha - \beta\alpha^*} \chi_\rho^z(\beta) \mathrm{d}^2\beta, \\ \chi_\rho^z(\beta) &= \text{tr}\left\{\hat{\rho}\hat{D}^z(\beta)\right\}, \text{ where } \hat{D}^z(\beta) = e^{z||\beta||^2/2} e^{\beta\hat{a}^\dagger - \beta^*\hat{a}}. \end{aligned} \tag{2–12}$$

In (2–12), z can be chosen from -1, 0 and 1. Different z will give a different phase space representation:

$$\begin{aligned} z = -1&\text{: Husimi function}^{[16]}; \\ z = 0&\text{: Wigner function}^{[17]}; \\ z = 1&\text{: Glauber-Sudarshan representation}^{[18]}. \end{aligned} \tag{2–13}$$

2.3.2 Fokker-Planck and Langevin equations

To investigate an open system in phase space, we introduce two types of dynamic equations: Fokker-Planck equation and stochastic Langevin equation. They are equivalent to each other and can represent a quantum system according to a master equation.

(1) Fokker-Planck equation

Here $P(\mathbf{x},t)$ is a time-dependent probability distribution for $\mathbf{x}$, a vector of variables with length N. The Fokker-Planck equation takes the form:

$$\partial_t P(\mathbf{x},t) = \left[-\sum_{j=1}^{N}\partial_j \mathbf{A}_j(\mathbf{x}) + \frac{1}{2}\sum_{j,l=1}^{N}\partial_j\partial_l \mathcal{D}_{jl}(\mathbf{x})\right]P(\mathbf{x},t), \tag{2–14}$$

where $\mathcal{D}(\mathbf{x}) \geq 0$ and $\mathcal{D}(\mathbf{x}) = \mathcal{D}^T(\mathbf{x})$. As $P(\mathbf{x},t)$ is a probability distribution, the average of an observable $f(\mathbf{x})$ is

$$\langle f(\mathbf{x})\rangle = \int_{\mathbb{C}^N} P(\mathbf{x},t) f(\mathbf{x}) \mathrm{d}^N\mathbf{x}. \tag{2–15}$$

(2) Stochastic Langevin equation

There is also a stochastic approach of writing a dynamic equation in phase space, which is simpler for numerical simulation. For a vector $\mathbf{x}$, the equation reads

$$\partial_t \mathbf{x} = \mathbf{A}(\mathbf{x}) + \mathcal{B}(\mathbf{x})\boldsymbol{\eta}(t), \tag{2–16}$$

where $\mathbf{A}(\mathbf{x})$ is a vector and $\mathcal{B}(\mathbf{x})$ is a gaussian noise matrix. $\boldsymbol{\eta}$ is a real noise vector, whose component satisfy $\overline{\eta_j(t)} = 0$ and $\overline{\eta_j(t)\eta_l(t')} = \delta_{jl}\delta(t-t')$. Here the overline represents stochastic average, which takes average of infinite trials. The stochastic noises are more rigorously defined with Wiener increment, whose introduction can be found in Schaffter et al.[19].

(3) Equivalence of two methods

It is possible to prove that Fokker-Planck and Langevin averages are equivalent, according to the connection

$$\begin{array}{ccc} \textbf{Fokker-Planck Eq.} & & \textbf{Langevin Eq.} \\ \mathbf{A};\ \mathcal{D} = \mathcal{B}\mathcal{B}^T & \Leftrightarrow & \mathbf{A};\ \mathcal{B} \end{array} \tag{2–17}$$

2.3.3 Positive P representation

Choosing $z = 1$ in (2–12) gives us the Glauber-Sudarshan P representation. For quantum systems, it generally leads $\mathcal{D}$ to be not positive semi-definite. To solve this problem, it is generalized to the so-called positive P representation, which introduces two independent complex variables for one mode, α and α^+. It is different from the standard Glauber-Sudarshan P representation, which depends on a single complex variable α. Master equation can be simply transformed to a equivalent Fokker-Planck equation and then we can obtain a stochastic equation for numerics. Let us introduce this more formally.

For a single mode system, $\mathbf{x} = (\alpha, \alpha^+)^T$, we define the probability distribution P_ρ^+ by

$$\begin{aligned} \chi_\rho^+(\beta,\beta^+) &= \mathrm{tr}\left\{\hat{\rho} e^{\beta\hat{a}^\dagger} e^{-\beta^+\hat{\alpha}}\right\} \\ &= \int_{\mathbb{C}^2} e^{\beta\alpha^+ - \beta^+\alpha} P_\rho^+(\alpha,\alpha^+). \end{aligned} \tag{2–18}$$

With this representation, observables $\langle \hat{a}^{\dagger m} \hat{a}^n \rangle$ can be calculated by

$$\begin{aligned} \langle \hat{a}^{\dagger m} \hat{a}^n \rangle &= (-1)^n \partial_\beta^m \partial_{\beta^+}^n \chi_\rho^+(\beta, \beta^+)\Big|_{\beta,\beta^+=0} \\ &= \int_{\mathbb{C}^2} P_\rho^+(\alpha, \alpha^+) \alpha^{+m} \alpha^n \mathrm{d}^2\alpha \mathrm{d}^2\alpha^+ \end{aligned} \tag{2–19}$$

To retrieve the state $\hat{\rho}$, we can follow Eq. (2–20)

$$\hat{\rho} = \int_{\mathbb{C}^2} P_\rho^+(\alpha, \alpha^+) \frac{|\alpha\rangle \langle \alpha^{+*}|}{\langle \alpha^{+*}|\alpha\rangle} \mathrm{d}^2\alpha \mathrm{d}^2\alpha^+ \tag{2–20}$$

With above properties, a transformation rule from master equation for Fokker-Planck equation is introduced in (2–21). For a master equation $\partial_t \hat{\rho} = \mathcal{L}[\hat{\rho}]$ and a Fokker-Planck equation $\partial_t P_\rho^+(\alpha, \alpha^+) = F(\alpha, \alpha^+) P_\rho^+(\alpha, \alpha^+)$, a map from $\mathcal{L}$ to $F(\alpha, \alpha^+)$ reads

$$\begin{array}{ccc} \mathcal{L} & & \mathbf{F}(\alpha, \alpha^+) \\ \hat{a}\hat{\rho} & \Leftrightarrow & \alpha \\ \hat{\rho}\hat{a} & \Leftrightarrow & \alpha - \partial_{\alpha^+} \\ \hat{a}^\dagger \hat{\rho} & \Leftrightarrow & \alpha^+ - \partial_\alpha \\ \hat{\rho}\hat{a}^\dagger & \Leftrightarrow & \alpha^+ \end{array} \tag{2–21}$$

Terms in master equation can be added and multiplied. For example, if $\hat{M} = \hat{\rho}\hat{a}^\dagger\hat{a}$, then $F = (\alpha - \partial_{\alpha^+})\alpha^+$.

After transforming master equation to a Fokker-Planck equation, the last step is applying (2–17) and obtaining a stochastic Langevin equation.

2.3.4 Stochastic simulation

Here we show a simple numerical method to integrate the stochastic equation, the mid-point integral method. We will explains it with the example of integrate $\mathbf{W}(T) = \int_0^T f(\mathbf{W}(t), t)dt$. At time t, the next increment over time interval Δt is calculated by:

$$\begin{aligned} \mathbf{W}_{mid} &= \mathbf{W}(t) + f(\mathbf{W}(t), t)\frac{\Delta t}{2} \\ \mathbf{W}(t + \Delta t) &= \mathbf{W}(t) + f\left(\mathbf{W}_{mid}, t + \frac{\Delta t}{2}\right)\Delta t \end{aligned} \tag{2–22}$$

The stochastic variable in $f(\mathbf{W}(t), t)$ are generated by pseudorandom algorithms at each iteration. Also, the time interval is determined automatically by keeping each term in $f(\mathbf{W}(t), t)$ lower than $\min(0.1\mathbf{W}(t))$. Setting a initial value and doing the iterative addition, we can get a final result. To obtain a statistical result, we need to perform this integration repeatedly, typically, for 2000 times. Then the stochastic average for observables can be performed.

2.4 Floquet method

In our research, we need to treat a periodically time-dependent differential equation, which is a linearized stochastic Langevin equation. Floquet theory was mainly proposed by Gaston Floquet[20], which has the power to solve this kind of problems. Consider a stochastic equation for $\mathbf{x}(t)$ of length D:

$$\frac{\mathrm{d}\mathbf{x}(t)}{\mathrm{d}t} = \mathcal{L}(t)\mathbf{x}(t) + \mathcal{B}(t)\boldsymbol{\xi}(t), \tag{2–23}$$

where $\mathcal{L}(t)$ (shape: $D \times D$) and $\mathcal{B}(t)$ (shape: $D \times N$) are periodical matrix with period T. $\xi(t)$ is a real stochastic vector of length N.

To solve it, we first define a principal fundamental matrix $\mathcal{F}(t)$ by

$$\frac{\mathrm{d}\mathcal{F}(t)}{\mathrm{d}t} = \mathcal{L}(t)\mathcal{F}(t), \text{ and } \mathcal{F}(0) = \mathcal{I}. \tag{2–24}$$

It's also called the propagator. In one period T, we construct a displacement matrix by $e^{\mathcal{M}T} = \mathcal{F}(T)$, and then counteract it in $\mathcal{F}(t)$:

$$\mathcal{P}(t) = \mathcal{F}(t)e^{-\mathcal{M}t}. \tag{2–25}$$

From (2–25) we obtain the Floquet normal form $\mathcal{P}(t)$, which is also a T-periodical matrix. Then we perform a variable change $\mathbf{s}(t) = \mathcal{P}^{-1}(t)\mathbf{x}(t)$, making Eq. (2–23) turns to

$$\frac{\mathrm{d}\mathbf{s}(t)}{\mathrm{d}t} = \mathcal{M}\mathbf{s}(t) + \mathcal{P}^{-1}(t)\mathcal{B}(t)\boldsymbol{\xi}(t), \tag{2–26}$$

by which we obtain a simple equation with a time-independent drifting term. We can normally solve it by diagonalizing $\mathcal{M}$.

But in this thesis, we will focus on the Floquet eigenvectors $\mathbf{p}_j$ and $\mathbf{q}_j^\dagger$ only, which is defined by

$$\begin{aligned} \mathcal{M}\mathbf{v}_j &= \mu_j\mathbf{v}_j, \text{ and } \mathbf{p}_j(t) = \mathcal{P}(t)\mathbf{v}_j \\ \mathbf{w}_j^\dagger\mathcal{M} &= \mu_j\mathbf{w}_j^\dagger, \text{ and } \mathbf{q}_j^\dagger(t) = \mathbf{w}_j^\dagger\mathcal{P}^{-1}(t) \end{aligned} \tag{2–27}$$

Note that in a physical system, all eigenvalues μ_j have negative real parts, except μ_0, which equals to zero. $\mathbf{p}_j$ and $\mathbf{q}_j^\dagger$ also satisfy orthogonality condition $\mathbf{q}_j^\dagger(\tau)\mathbf{p}_l(\tau) = \delta_{jl}$.

Chapter 3 Implementation of the Van der Pol model with superconducting circuits

3.1 Architecture with superconducting circuits

Classically, a Van der Pol system is a non-conservative oscillator with non-linear damping proposed by Van der Pol[7]. In this section, we give a general version of a quantum Van der Pol model in (3–1) and manage to construct it with superconducting circuits.

$$\partial_t \hat{\rho} = -i\left[\Delta \hat{a}^\dagger \hat{a} + \left(\epsilon \hat{a}^\dagger + H.c.\right), \hat{\rho}\right] + \gamma \mathcal{D}_{\hat{a}^\dagger}[\hat{\rho}] + \kappa \mathcal{D}_{\hat{a}^2}[\hat{\rho}] \tag{3–1}$$

Here Δ is the detuning between the driving frequency and the intrinsic one, and ϵ is the driving amplitude. As shown in the master equation, apart from the conventional Hamiltonian part, the Van der Pol model contains a incoherent pumping and two-photon dissipation of rates γ and κ, respectively.

To implement the Van der Pol model, we propose a multi-mode generalization of the Asymmetrically Threaded SQUID (ATS) system introduced by Lescanne et al.[15]. Its generalized Hamiltonian has a third-order coupling term $\epsilon(t)\left(\sum_{j=1}^{N} \hat{\varphi}_j\right)^3$, with which we can achieve down-conversion on multiple modes and get two-photon loss.

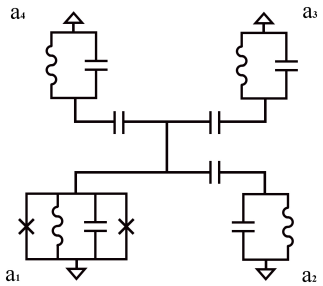

Figure 3–1 The construction of a Van der Pol oscillator.

We coupled an ATS circuit and 3 cat modes to build our model in Figure 3–1, and finally the whole system will behave as a Van der Pol oscillator with down conversion. These modes are named from a_1 to a_4, and a_1 is an ATS mode. For each of the mode a_j, its frequency is ω_j. They are all open systems coupled with the environment at $0K$. Also, we drive a_1 and a_4 with frequency ν_1 and

ν_4. This four-wave mixing system is described by the master equation:

$$\begin{aligned}
&\partial_t\hat{\rho} = -i[\hat{H}_0, \hat{\rho}] + \sum_{j=1}^{4} \gamma_j \mathcal{D}_{\hat{a}_j}[\hat{\rho}], \\
&\text{where } \hat{H}_0 = \sum_{j=1}^{4} \omega_j \hat{a}_j^\dagger \hat{a}_j + 2E_J\epsilon_0 \left[\sum_{j=1}^{4} \hat{\varphi}_j - \frac{1}{6}\left(\sum_{j=1}^{4} \hat{\varphi}_j\right)^3\right] \\
&\qquad + \left(\epsilon_1 e^{-i\nu_1 t}\hat{a}_1^\dagger + \epsilon_4 e^{-i\nu_4 t}\hat{a}_4^\dagger + H.c.\right).
\end{aligned} \tag{3–2}$$

To successfully realize down conversion, we manually select $\omega_3 \approx 2\omega_1$, $\omega_4 \approx \omega_1 + \omega_2$, $\nu_1 \approx \omega_1$ and $\nu_4 \approx \omega_4$.

3.2 Effective single-mode system

In this section, we will prove that this four-mode system behaves effectively as a Van der Pol oscillator.

3.2.1 Change of pictures

We first cancel the driven term in the Hamiltonian with a time-independent displacement $\hat{D}_{j,0} = e^{\alpha_{j,0}\hat{a}_j^\dagger - \alpha_{j,0}^*\hat{a}_j}$ for each $\hat{a}_j$. To fully eliminate the stable $\hat{a}_j$ terms, we choose $\alpha_{j,0} = 2E_J\epsilon_0/(\omega_j - i\gamma_j)$. The state $\hat{\rho}_{D,0} = \hat{D}_{j,0}^\dagger \hat{\rho} \hat{D}_{j,0}$ in the new picture evolves according to the master equation:

$$\begin{aligned}
&\partial_t\hat{\rho}_{D,0} = -i[\hat{H}_{D,0}, \hat{\rho}_{D,0}] + \sum_{j=1}^{4} \gamma_j \mathcal{D}_{\hat{a}_j}[\hat{\rho}_{D,0}], \\
&\text{where } \hat{H}_{D,0} = \sum_{j=1}^{4} \omega_j \hat{a}_j^\dagger \hat{a}_j + \frac{1}{3}E_J\epsilon_0 \left[\sum_{j=1}^{4} \left(\varphi_j \hat{a}_j + \varphi\alpha_{j,0} + H.c.\right)\right]^3 \\
&\qquad + \left(\epsilon_1 e^{-i\nu_1 t}\hat{a}_1^\dagger + \epsilon_4 e^{-i\nu_4 t}\hat{a}_4^\dagger + H.c.\right).
\end{aligned} \tag{3–3}$$

The rotating displacement has not been eliminated in this step.

With ω_j much larger than any other parameters, we can move to a rotating frame and use rotating wave approximation to eliminate the high-frequency terms. The transformation we use is $\hat{U}_R = e^{-i[\nu_1\hat{a}_1^\dagger\hat{a}_1 + (\nu_4-\nu_1)\hat{a}_2^\dagger\hat{a}_2 + 2\nu_1\hat{a}_3^\dagger\hat{a}_3 + \nu_4\hat{a}_4^\dagger\hat{a}_4]}$, so that $\hat{\rho}_R = \hat{U}_R^\dagger\hat{\rho}_{D,0}\hat{U}_R$ evolves according to the master equation:

$$\begin{aligned}
&\partial_t\hat{\rho}_R = -i[\hat{H}_R, \hat{\rho}_R] + \sum_{j=1}^{4} \gamma_j \mathcal{D}_{\hat{a}_j}[\hat{\rho}_R], \\
&\text{where } \hat{H}_R = \sum_{j=1}^{4} \Delta_j \hat{a}_j^\dagger \hat{a}_j + \left(\epsilon_1\hat{a}_1 + \epsilon_4\hat{a}_4 + g_3\hat{a}_3\hat{a}_1^{\dagger 2} + g_4\hat{a}_4\hat{a}_1^\dagger\hat{a}_2^\dagger + H.c.\right)
\end{aligned} \tag{3–4}$$

Here Δ_j is the detuning between inherent frequency and driving frequency: $\Delta_1 = \omega_1 - \nu_1$, $\Delta_2 = \omega_2 + \nu_1 - \nu_4$, $\Delta_3 = \omega_3 - 2\nu_1$ and $\Delta_4 = \omega_4 - \nu_4$. We have also defined the down-conversion rates: $g_3 = E_J\epsilon_0\varphi_3\varphi_1^{*2}$ and $g_4 = 2E_J\epsilon_0\varphi_4\phi_1^*\varphi_2^*$. After rotating wave approximation, the coupling terms clearly shows that down conversion happens. Term $\hat{a}_3\hat{a}_1^{\dagger 2}$ means that a photon in mode a_3 can

transmit into a_1's two photons, and similarly, term $\hat{a}_4\hat{a}_1^\dagger\hat{a}_2^\dagger$ means one annihilation in mode a_4 will result in creation in both a_1 and a_2.

For this rotating frame, we finally eliminate the rotating displacement for $\hat{a}_4$. Using transformation $\hat{U}_D = e^{\alpha_4\hat{a}_4 - H.c.}$ and $\alpha_4 = \epsilon_4/(\Delta_4 - i\gamma_4)$, we move to the final picture, where $\hat{\rho}_D = \hat{U}_D^\dagger\hat{\rho}_R\hat{U}_D$ evolves as:

$$\begin{aligned}
&\partial_t\hat{\rho}_D = -i[\hat{H}_D, \hat{\rho}_D] + \sum_{j=1}^{4}\gamma_j\mathcal{D}_{\hat{a}_j}[\hat{\rho}_D],\\
&\text{where } \hat{H}_D = \sum_{j=1}^{4}\Delta_j\hat{a}_j^\dagger\hat{a}_j + \left(\epsilon_1\hat{a}_1 + g_3\hat{a}_3\hat{a}^{\dagger 2} + g_4\hat{a}_4\hat{a}_1^\dagger\hat{a}_2^\dagger + g_4\alpha_4\hat{a}_1^\dagger\hat{a}_2^\dagger + H.c.\right).
\end{aligned} \tag{3–5}$$

3.2.2 Eliminate $\hat{a}_3$ and $\hat{a}_4$

We tune γ_4 and γ_3 larger than other parameters, result in a_3 and a_4 cooled by the environment. We can treat them as irrelevant modes and use effective theory in Section 2.2 to eliminate them. We separate the master equation $\partial_t\hat{\rho}_D = \mathcal{L}[\hat{\rho}_D]$ into $\mathcal{L} = \mathcal{L}_0 + \mathcal{L}_1 = \mathcal{L}_S + \mathcal{L}_E + \mathcal{L}_1$, and

$$\begin{aligned}
\mathcal{L}_S[\hat{\rho}_D] =& -i\left[\Delta_1\hat{a}_1^\dagger\hat{a}_1 + \Delta_2\hat{a}_2^\dagger\hat{a}_2 + \left(\epsilon\hat{a}_1^\dagger + g_4\alpha_4\hat{a}_1^\dagger\hat{a}_2^\dagger + H.c.\right), \hat{\rho}_D\right]\\
&+ \gamma_1\mathcal{D}_{\hat{a}_1}[\hat{\rho}_1] + \gamma_2\mathcal{D}_{\hat{a}_2}[\hat{\rho}_2],\\
\mathcal{L}_E[\hat{\rho}_D] =& -i\left[\Delta_3\hat{a}_3^\dagger\hat{a}_3 + \Delta_4\hat{a}_4^\dagger\hat{a}_4, \hat{\rho}_D\right] + \gamma_3\mathcal{D}_{\hat{a}_3}[\hat{\rho}_3] + \gamma_4\mathcal{D}_{\hat{a}_4}[\hat{\rho}_4],\\
\mathcal{L}_1[\hat{\rho}_D] =& -i\left[g_3\hat{a}_3\hat{a}_1^{\dagger 2} + g_4\hat{a}_4\hat{a}_1^\dagger\hat{a}_2^\dagger + H.c., \hat{\rho}_D\right].
\end{aligned} \tag{3–6}$$

With effective theory, mode a_3 and a_4 are eliminated, the master equation for reduced state $\hat{R}_R^{12} = \mathrm{tr}_{3,4}\left\{\hat{\rho}_D\right\}$.

$$\begin{aligned}
&\partial_t\hat{\rho}_R^{12} = -i\left[\hat{H}_R^{12}, \hat{\rho}_R^{12}\right] + \sum_{j=1}^{2}\gamma_j\mathcal{D}_{\hat{a}_j}[\hat{\rho}_R^{12}] + \kappa_{12}\mathcal{D}_{\hat{a}_1\hat{a}_2}[\hat{\rho}_R^{12}] + \kappa_1\mathcal{D}_{\hat{a}_1^2}[\hat{\rho}_R^{12}],\\
&\text{where } \hat{H}_R^{12} = \sum_{j=1}^{2}\Delta_j\hat{a}_1^\dagger\hat{a}_1 + \left(\epsilon_1\hat{a}_1^\dagger + g_4\alpha_4\hat{a}_1^\dagger\hat{a}_2^\dagger + H.c.\right)\\
&\qquad + u_1\hat{a}_1^{\dagger 2}\hat{a}_1^2 + u_{12}\hat{a}_1^\dagger\hat{a}_2^\dagger\hat{a}_1\hat{a}_2,\\
&\kappa_1 = \frac{g_3^2\gamma_3}{\Delta_3^2+\gamma_3^2},\ \kappa_{12} = \frac{g_4^2\gamma_4}{\Delta_4^2+\gamma_4^2},\ u_1 = \frac{g_2^2\Delta_3}{\Delta_3^2+\gamma_3^2},\ u_{12} = -\frac{g_4^2\Delta_4}{\Delta_4^2+\gamma_4^2}.
\end{aligned} \tag{3–7}$$

3.2.3 Eliminate $\hat{a}_2$

Next we choose γ_2 much larger than other parameters and eliminate mode a_2 with the same technique. Finally we get an effective system for a_1, whose reduced state $\hat{\rho}_R^1 = \mathrm{tr}_2\left\{\hat{\rho}_R^{12}\right\}$ follows the evolution function:

$$\begin{aligned}
&\partial_t\hat{\rho}_R^1 = -i\left[\hat{H}_R^1, \hat{\rho}_R^1\right] + \gamma_1\mathcal{D}_{\hat{a}_1}[\hat{\rho}_R^1] + \Gamma_1\mathcal{D}_{\hat{a}_1^\dagger}[\hat{\rho}_R^1] + \kappa_1\mathcal{D}_{\hat{a}_1^2}[\hat{\rho}_R^1],\\
&\text{where } \hat{H}_R^1 = \delta_R\hat{a}_1^\dagger\hat{a}_1 + \left(\epsilon_1\hat{a}_1^\dagger + H.c.\right) + u_1\hat{a}_1^{\dagger 2}\hat{a}_1^2,\\
&\delta_R = \Delta_1 - \frac{||g_4\alpha_4||^2}{\gamma_2^2+\Delta_2^2}\Delta_2,\ \Gamma_1 = \frac{||g_4\alpha_4||^2}{\gamma_2^2+\Delta_2^2}\gamma_2.
\end{aligned} \tag{3–8}$$

Eq. (3–8) is our final equation for the effective system. The characteristic damping terms $\Gamma_1 \mathcal{D}_{\hat{a}_1^\dagger}[\hat{\rho}_R^1]$ and $\kappa_1 \mathcal{D}_{\hat{a}_1^2}[\hat{\rho}_R^1]$ shows that it is a Van der Pol oscillator. With precisely controlling the parameters, we now are able to build a Van der Pol system with controllable detuning, driving and damping.

Chapter 4 A single Van der Pol oscillator

4.1 Classical Limit

In section 3.2, we built a VdP oscillator with superconducting circuit system. According to (3–8), the master equation reads:

$$\begin{aligned} &\partial_t \hat{\rho} = -i\left[\hat{H}, \hat{\rho}\right] + \gamma D_a\left[\hat{\rho}\right] + \kappa D_{a^2}\left[\hat{\rho}\right] + \Gamma D_{a^\dagger}\left[\hat{\rho}\right], \\ &\text{where } \hat{H} = \delta \hat{a}^\dagger \hat{a} + \left(\epsilon \hat{a}^\dagger + H.c.\right) + u\hat{a}^{\dagger 2}\hat{a}^2. \end{aligned} \tag{4–1}$$

We first investigate our model classically by assuming the state is a coherent at all tiems, $|\alpha(t)\rangle$. With $\langle \hat{a}^{\dagger m}\hat{a}^n\rangle = \alpha^{*m}\alpha^n$, we can find the evolution equation for the displacement. This leads to the classical limit of our Van der Pol system:

$$\partial_t \alpha = -i\epsilon + \left[-i\delta + \Gamma - \gamma - 2\left(\kappa + iu\right)|\alpha|^2\right]\alpha \tag{4–2}$$

In the following, we set $u = 0$, and change to dimensionless variables $\tau = (\Gamma - \gamma)t$ and $\beta = \sqrt{\frac{2\kappa}{\Gamma-\gamma}}\alpha$, we absorbed Γ and γ into the observables. Defining $F = \frac{-i\epsilon\sqrt{2\kappa}}{(\Gamma-\gamma)^{3/2}}$ and $\Delta = -\frac{\delta}{\Gamma-\gamma}$, this is the final form of the classical equation:

$$\partial_\tau \beta = F + \left(i\Delta + 1 - |\beta|^2\right)\beta, \tag{4–3}$$

which depends only on two dimensionless parameters, the effective driving amplitude F and the normalized detuning Δ.

4.2 Phase diagram of classical model

With different parameters, a classical Van der Pol oscillator has different dynamic behaviors. Apart from having stable solutions, it runs in limit cycle in special conditions. A limit cycle is a closed trajectory in phase space as time approaches infinity, which makes it useful and famous across the industry and scientific research. Such a dynamical evolution is also a good candidate for time crystals. A typical limit cycle in our model is displayed in Figure 4–1. We plot the periodical behavior of β versus time in Figure 4–1a. Also, its limit cycle is shown in Figure 4–1b, where we plot Im(β) versus Re(β).

Navarrete-Benlloch et al.[10] introduce the phase diagram of a Van der Pol model. With their approach, we first acquire the asymptotic state by setting the right hand side of Eq. (4–3) to 0. It lead to an equilibrium equation for the oscillator's intensity $I = |\beta|^2$.

$$F^2 = \left(\Delta^2 + 1\right)I - 2I^2 + I^3 \tag{4–4}$$

Also, they investigated the stability of these steady states with the linear stability matrix. Finally, Figure 4–2 shows the phase diagram for it. The dynamic equation has two independent parameters in total: F and Δ. By choosing different parameters, we find the model has five different phases,

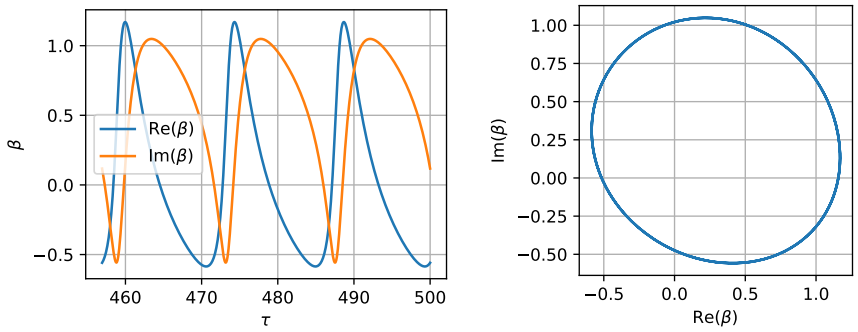

a) Three periods of β versus time

b) Limit cycle in phase space

Figure 4–1 Periodical behavior in limit cycle phase

represented by different colors in the figure. Sub figures are plotted with different Δ. In each sub figure, the amplitude I of possible solutions of the oscillator is plotted versus the driving F. Stable stationary solutions are plotted with solid lines, and unstable solutions are plotted with dashes lines. We also show the time-periodic solutions (limit cycles), displayed with dots and bars. The dots shows the time average of $|\beta|^2$, and bars indicate the standard deviation of such dynamic evolution in one period.

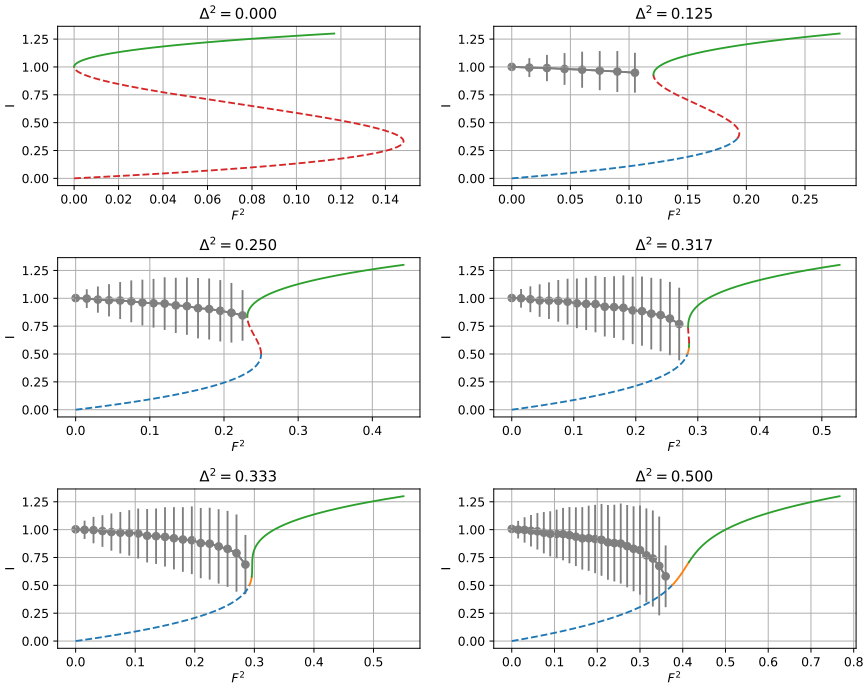

Figure 4–2 Phase diagram

According to the figure, if detuning Δ is not 0, limit cycle phase appears on the phase diagram. As Δ increases, the limit cycle phase has larger range for F.

4.3 Liouvillian spectrum of quantum Van der Pol model

It's known that typically an open quantum system has only one stable state, or in another word, the Liouvillian in master equation has only one zero eigenvalue. However, as we shown classically, the Van der Pol oscillator has different phases with different numbers of stable states. For example, in Figure 4–2, we can easily find parameters corresponding to one or two stable states. Moreover, a model in limit cycle phase has infinitely-many dynamically stable states. In this section, we will unveil the classical-quantum transition through the spectrum of the quantum model.

We do a similar parameter change as the classical version: $u = 0$, $\tau = (\Gamma - \gamma)t$, $F = \frac{-i\epsilon\sqrt{2\kappa}}{(\Gamma-\gamma)^{3/2}}$, $\Delta = -\frac{\delta}{\Gamma-\gamma}$ and $\kappa' = \frac{2\kappa}{\Gamma-\gamma}$. For simplicity, we also set $\gamma = 0$ and $\Gamma = 1$. The master equation for quantum Van der Pol model becomes:

$$\partial_\tau \hat{\rho} = \left[i\Delta \hat{a}^\dagger \hat{a} + \left(\frac{F}{\sqrt{\kappa'}} \hat{a}^\dagger - H.c. \right), \hat{\rho} \right] + \mathcal{D}_{\hat{a}^\dagger}[\hat{\rho}] + \frac{\kappa'}{2} \mathcal{D}_{\hat{a}^2}[\hat{\rho}] \tag{4–5}$$

Look back to what we do in Section 4.1, we absorb the dissipative parameter κ' into α, by using $\beta = \sqrt{2\kappa'}\alpha$. It result in a equation without κ'. In this way, we can actually control how classical the model is by changing κ'. We can observe it from the displacement. For the same β, a smaller κ' gives a larger α. So when κ' is smaller, the Van der Pol system contains more coherent photons and it is more classical. We will show this by plotting three examples.

We vectorize the state with Fock basis truncated up to $N = 400$ and flatten the $\hat{\rho}$ matrix to a vector of length $(N+1)^2$. The Liouvillian can be represented by a sparse matrix with shape $(N+1)^2 \times (N+1)^2$[21]. Setting $\Delta = 0.3167$ and selecting different F, we investigate in the eigenvalues of the super operator when κ' changes. Typical eigen-spectra of the Liouvillian are plotted in the Figure 4–3. We place the eigenvalues as dots on the complex plane, and different colors represent different κ'.

Figure 4–3a shows the spectrum in classical limit cycle phase ($\Delta^2 = 0.3167$ and $F^2 = 0.2$). Focusing on a series of eigenvalues, say, the purple dots ($\kappa' = 0.020$), the spectrum form a approximately horizontal curve at the top of the figure. The Liouvillian has a list of eigenvalues with small real parts. Empirically, in this phase, real parts of the eigenvalues become closer to zero when κ' goes to zero. These states are asymptotically becoming dynamically stable states when the system become more classical, and there will be infinity of them. It indicates that the model will have infinite classical stable states, corresponding to the classical limit cycle behavior.

In Figure 4–3b, we display the classical stable phase($\Delta^2 = 0.3167$ and $F^2 = 0.35$). The figure shows the imaginary parts of the eigenvalues become zero when κ' goes to zero, which becomes significant when κ' is less than 0.02. And in this phase, only one stable eigenstate have zero real part, which means only one state will survive.

Figure 4–3c displays the classical bifurcation phase, where classical VdP oscillator has two stable solutions. Quantum mechanically, when κ' gets smaller, the system will have three eigenvalues close to zero. We believe that the two non-zero eigenvalues will meet at the vertical axis when $\kappa' \to 0$. We will roughly exhibit such behaviors in 4–4. In a word, the classical bifurcation corresponds to the original stable state plus one of the non-zero eigenvalues, which approaches 0 as $\kappa' \to 0$.

Figure 4–4 shows the spectrum pattern with the change of F. With $\Delta = 0.317$ and $\kappa' = 0.01$,

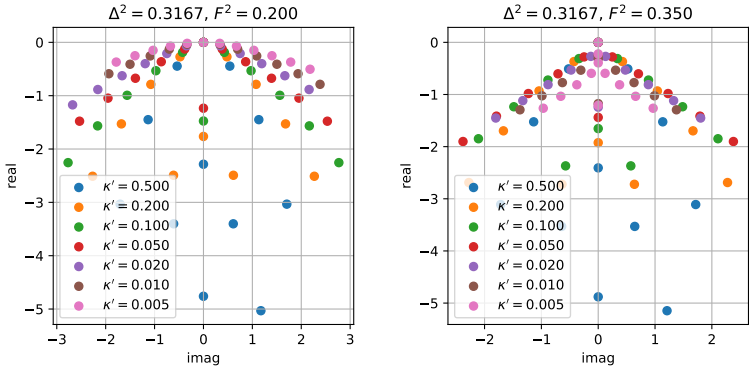

a) Limit cycle phase b) Stable phase

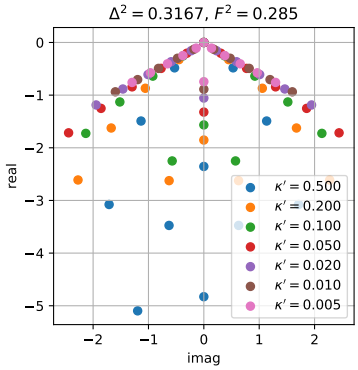

c) Bifurcation phase

Figure 4–3 Typical spectrum of the Liouvillian

we observe a pattern change at around $F^2 = 0.35$, where the second and the third eigenvalues merge at the axis. Although this point have no correspondence classically in this phase, but it may related to the formation of the bifurcation.

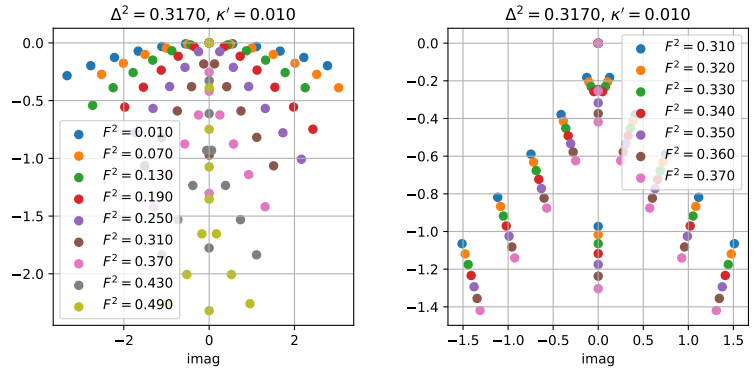

a) From $F = 0.01$ to $F = 0.49$ b) From $F = 0.31$ to $F = 0.37$

Figure 4–4 Spectrum with different F

4.4 Quantum non-equilibrium behavior: time-crystalline order?

For a classical Van der Pol oscillator in limit cycle phase, it oscillates with a certain phase continuously. Since the dynamical equation has time translational symmetry, the classical oscillator experience a Spontaneous Symmetry Breaking (SSB). However, such a classical system requires $\kappa' \to 0$ to achieve infinite excitations, which is impossible in real world. Moreover, for any non-vanishing κ' ,we will show that quantum fluctuations end up destroying the symmetry breaking state and turn it into one that preserves time-translational invariance. Hence, time-crystalline order is not possible in a single Van der Pol oscillator, since it is not robust against quantum fluctuations.

Achieving a continuously oscillating system with SSB is difficult in quantum mechanics. The system is not only disturbed by the quantum noise, but also effected by the non-equilibrium dynamics. Since the oscillating state is far from equilibrium, the quantum Van der Pol oscillator will inevitably fall into a steady state in the end, which is just a matter of time for a simple quantum open system. We investigate in this non-equilibrium system via two method, direct visualization and approximate analytical calculation. For simplicity, we use a non-driven system as an example, where $F = 0$ and $\Delta = 0.26$. Here the non-zero Δ doesn't come from detuning but from an inherent frequency.

4.4.1 Direct visualization

First, we show the Wigner visualization of the non-equilibrium evolution in Figure 4–5. Initially, the system is in a coherent state. Via vectorizing the state in Fock basis and integrating the master equation, we simulate the Van der Pol system with $\kappa' = 0.12$, from $\tau = 0$ to $\tau = 28$.

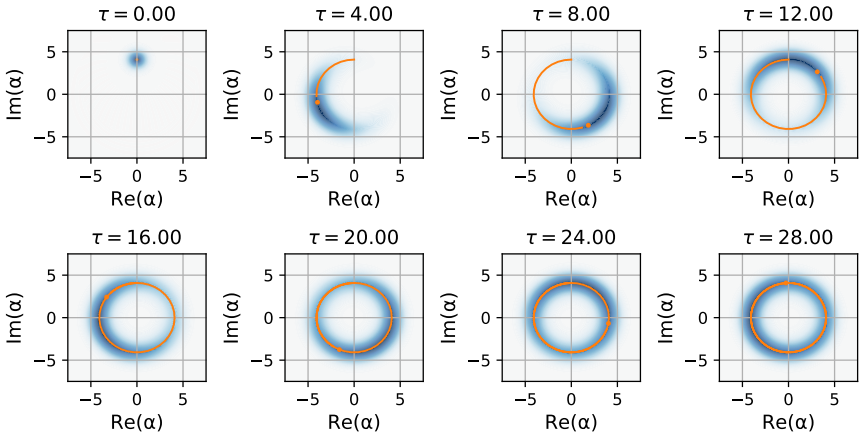

Figure 4–5 Wigner visualization

Clearly in Figure 4–5, in finite time, a coherent state will gradually diffuse to a uniform steady state, which looks like a blue ring in the phase space. Such a steady state will not oscillate anymore and end the time crystal behavior. When quantum noises pull the system's phase apart from the original phase randomly, the system can't correct such deviation and result in phase diffusion.

4.4.2 Analysis

Luckily, we are able to show this phase diffusion effect analytically. Using positive-P representation introduced in Section 2.3, the system is described by a vector $\boldsymbol{\beta} = \left(\beta, \beta^+\right)^T$. Its evolution follows a stochastic equation set:

$$\begin{aligned} &\partial_\tau \boldsymbol{\beta} = \mathbf{A}(\boldsymbol{\beta}) + \mathcal{B}(\boldsymbol{\beta})\boldsymbol{\eta}(\tau), \\ &\text{where } \mathbf{A}(\boldsymbol{\beta}) = \begin{pmatrix} F + \beta\left(i\Delta + 1 - \beta^+\beta\right) \\ F + \beta^+\left(-i\Delta + 1 - \beta^+\beta\right) \end{pmatrix}, \\ &\mathcal{B}(\boldsymbol{\beta}) = \sqrt{\kappa'}\begin{pmatrix} i\beta & 0 & 1 & i \\ 0 & -i\beta^+ & 1 & -i \end{pmatrix} \end{aligned} \tag{4–6}$$

$\boldsymbol{\eta}(\tau)$ is a real stochastic vector of length 4.

Following Navarrete-Benlloch et al.[10], we linearize the system around limit cycle, assuming the fluctuation b is small compared to the classical motion:

$$\begin{aligned} \beta(\tau+\theta) &= \bar{\beta}(\tau+\theta) + b(\tau+\theta) \\ \beta^+(\tau+\theta) &= \bar{\beta}^*(\tau+\theta) + b^+(\tau+\theta) \end{aligned} \tag{4–7}$$

Here $\bar{\beta}(\tau+\theta)$ is the classical solution of (4–3) and θ describes the phase shift from the classical trajectory. Applying (4–7) to (4–6), we get a linearized equation

$$\partial_\tau \mathbf{b}(\tau) + \mathbf{p}_0(\tau)\partial_\tau\theta(\tau) = \mathcal{L}(\tau)\mathbf{b}(\tau) + \sqrt{\kappa'}\mathbf{n}(\tau), \tag{4–8}$$

where $\mathbf{b} = (b, b^+)^T$, $\mathbf{p}_0 = (\partial_\tau\bar{\beta}, \partial_\tau\bar{\beta}^*)^T$, $\mathbf{n} = \left[\sqrt{2}\xi - i\bar{\beta}\eta, \sqrt{2}\xi^* - i\bar{\beta}\eta^+\right]^T$. ξ is a complex stochastic variable, η and η^+ are the real ones. Linear stability matrix $\mathcal{L}$ reads

$$\mathcal{L}(\tau) = \begin{pmatrix} 1 - 2|\bar{\beta}(\tau)|^2 + i\Delta & -\bar{\beta}(\tau)^2 \\ -\bar{\beta}^{*2}(\tau) & 1 - 2|\bar{\beta}(\tau)|^2 - i\Delta \end{pmatrix}. \tag{4–9}$$

The noise term can be described by the correlation $\overline{n_j(\tau)n_l(\tau')} = N_{jl}(\tau)\delta\left(\tau - \tau'\right)$, and

$$\mathcal{N}(\tau) = \begin{pmatrix} -\bar{\beta}^2(\tau) & 2 \\ 2 & -\bar{\beta}^{*2}(\tau) \end{pmatrix}. \tag{4–10}$$

To solve the periodic dynamic equation, the Floquet method is used, introduced in Section 2.4. We will make use of left and right Floquet eigenvectors $\mathbf{p}_j(\tau)$ and $\mathbf{q}_j^\dagger(\tau)$, which satisfy

$$\begin{aligned} \dot{\mathbf{p}}_j(\tau) &= \left[\mathcal{L}(\tau) - \mu_j\right]\mathbf{p}_j(\tau), \\ \dot{\mathbf{q}}_j^\dagger(\tau) &= \mathbf{q}_j^\dagger(\tau)\left[\mu_j - \mathcal{L}(\tau)\right]. \end{aligned} \tag{4–11}$$

Also, the left eigenvectors and right ones satisfy the orthogonality conditions $\mathbf{q}_j^\dagger(\tau)\mathbf{p}_l(\tau) = \delta_{jl}$.[10] proved that $\mathbf{p}_0$ in (4–8) is exactly the Floquet right eigenvector corresponding to the zero eigenvector.

Now we apply $\mathbf{q}_0^\dagger$ to the left side of (4–8), obtaining $\partial_\tau\theta = \sqrt{\gamma}\mathbf{q}_0^\dagger(\tau)\mathbf{n}(\tau)$. Here we have remove a redundant term $\mathbf{q}_0^\dagger\mathbf{b}$ off by setting it to zero. Finally the integration can be carried out:

$$V(\tau) = \overline{[\theta(\tau) - \theta(0)]^2} = \gamma\int_0^\tau d\tau' \mathbf{q}_0^\dagger\left(\tau'\right)\mathcal{N}\left(\tau'\right)\mathbf{q}_0^*\left(\tau'\right) \tag{4–12}$$

For a non-driven system, Eq. (4–3) has an analytical solution: $\bar{\beta} = e^{i\Delta t+\phi}$, where ϕ is an arbitrary initial phase. Plugging it in (4–10) and (4–12), we obtain $V(\tau) = \frac{3}{2}\kappa'\tau$, a linearly increasing variance with slope $s_0 = \frac{3}{2}\kappa'$. It means that the phase diffuses continuously within our linearization approximations.

We perform a stochastic simulation of (4–6) to verify this result, using the mid-point method introduced in Section 2.3.4. In this simulation, we set $F = 0$, $\Delta = 0.26$, $\kappa' = 10^{-6}$ and simulate the system between $\tau = 0$ and $\tau = 20$ for 2000 stochastic trajectories. At every time step τ_x, we calculate the phase $\theta(\tau_x)$ by $\theta(\tau_x) = \mathrm{Im}\left[\ln(\beta(\tau_x)/\bar{\beta}(\tau_x))\right]$. We then evaluate the variance of phase $\theta(\tau_x)$ over stochastic repetitions. The variance is divided by a slope s_0 and finally plotted on Figure 4–6. It shows that our analytical prediction is true, and the variance of the system experiences a linear growth.

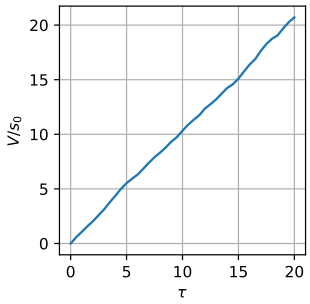

Figure 4–6 Variance growth

In a word, we are not able to protect time-crystalline order through a single Van der Pol oscillator because of quantum fluctuation. Such an oscillating system will not last long and become equilibrium in the end.

Chapter 5 Time-crystalline order in Van der Pol lattices

5.1 Coupled Van der Pol lattice

Lee et al.[9] show that coupling Van der Pol oscillators together will exhibit phase lock phenomena. Our classical simulation in Section B also give some examples of this by several numerical experiments. To protect the oscillation against quantum noise, we propose to build coupled Van der Pol lattices. L coupled Van der Pol oscillators are described by a master equation:

$$\begin{aligned} &\partial_t \hat{\rho} = -i\left[\hat{H}, \hat{\rho}\right] + \sum_{j=0}^{L-1}\left(D_{a_j}[\hat{\rho}] + \frac{\kappa'}{2} D_{a_j^2}[\hat{\rho}]\right), \\ &\text{where } \hat{H} = \sum_{j=0}^{L-1}\left[-\Delta \hat{a}_j^\dagger \hat{a}_j + \left(-i\frac{F}{\sqrt{\kappa'}}\hat{a}_j^\dagger + H.c.\right) + i\frac{g}{N_c}\hat{a}_j^\dagger \sum_{c_j} \hat{a}_{c_j}\right]. \end{aligned} \tag{5–1}$$

The last summation is over all modes $\hat{a}_{c_j}$ that are coupled with $\hat{a}_j$. N_c is the connectivity of the system, representing how many oscillators a mode is connected to. For example, lattice of dimension D has connectivity $N_c = 2D$. g is a real coupling constant, and it is divided by the connectivity, which keeps the Hamiltonian extensive in the system size.

Similar to Section 4.4.2, we focus on the non-driven system for simplicity. With $\Delta = 0$ and $F = 0$, a non-driven Van der Pol lattice is simple enough for us to investigate in its classical analytical solution. (5–1) is equivalent to a stochastic equation (5–2) using positive P representation. For each mode β_j:

$$\begin{aligned} \partial_\tau \beta_j &= \left(1 - \beta_j^+ \beta_j\right)\beta_j + i\frac{g}{N_c}\sum_{c_j}\beta_c + \sqrt{\kappa'}\left[\sqrt{2}\xi_j(\tau) + i\beta_j\eta_j(\tau)\right] \\ \partial_\tau \beta_j^+ &= \left(1 - \beta_j^+ \beta_j\right)\beta_j^+ - i\frac{g}{N_c}\sum_{c_j}\beta_c^+ + \sqrt{\kappa'}\left[\sqrt{2}\xi_j^*(\tau) - i\beta_j^+\eta_j^+(\tau)\right] \end{aligned} \tag{5–2}$$

ξ_j are complex gaussian noises, η_j and η_j^+ are real gaussian noises.

5.2 Stability of 1D Van der Pol ring

In this section, we focus on 1D Van der Pol ring as an example, which means mode j is only coupled with mode $j-1$ and $j+1$. Note that when j of some mode is less than 0 or larger than $L-1$, we regard it as j mod L. Oscillators at head and tail are coupled, make this system a ring.

5.2.1 Patterns of the solutions

Setting $\kappa' = 0$ and solving (5–2), we can get the a set of classical solutions and find the patterns of steady states. Oscillators from all these states shares the same limit cycle, circle of radius 1, with different in phases.

$$\bar{\beta}_j(\tau) = e^{2\pi i jk/L + 2ig_k\tau + i\theta}, \quad g_k = g\cos(2\pi k/L). \tag{5–3}$$

Here k represents different stable pattern of the system. For a certain pattern, modes with different phases are arranged in order, and if k is a factor of L, a sub-pattern appears on the ring repeatedly. Here we define l to be the number of distinct phases that $\bar{\beta}_j$ can have, which is also the least oscillator number of the sub-pattern. For example, when we choose $k = L/3$, $l = 3$. The phases of oscillators are: $0, \frac{2\pi}{3}, \frac{4\pi}{3}, 0, \frac{2\pi}{3}, \cdots$. By scattering all β_j in one complex plane, Figure 5–1 displays some different patterns. It should be noted that, solutions in (5–3) don't cover all stable patterns.

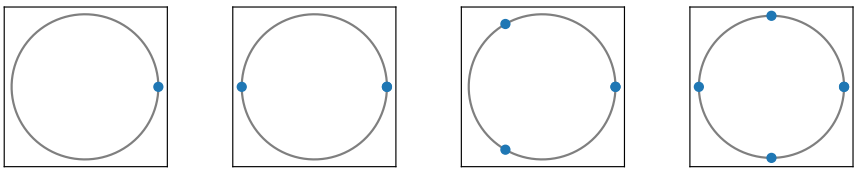

a) $l = 1$ b) $l = 2$ c) $l = 3$ d) $l = 4$

Figure 5–1 Different patterns of stable solutions

Besides, Eq. (5–3) shows that each mode is rotating with frequency g_k, which comes from the coupling effect with neighbors.

5.2.2 Stability analysis

It can be analytically proved and numerically tested that, all these patterns with different k are stables solution of (5–2). Following is the proof:

Linearization To investigate in the stability, we only need to focus on the classical part of the (5–2). The system is described by $\boldsymbol{\beta} = \left(\beta_1, \beta_1^+, \cdots, \beta_L, \beta_L^+\right)$ with positive P representation. Similar to the way we obtain (4–8), it is linearized via $\boldsymbol{\beta}(\tau + \theta) = \bar{\boldsymbol{\beta}}(\tau + \theta) + \mathbf{b}(\tau + \theta)$ and finally it can be described by (5–4). Importantly, all modes share the same θ because of the coupled system is only invariant under global time translations, not translations of each oscillators independently, which will be discussed later in Section 5.4. Note that, in the following all superscripts represent the size of the subsystem. For example, $\mathcal{L}^L(\tau)$ is a $(2L \times 2L)$ matrix. We obtain:

$$
\begin{aligned}
&\partial_\tau \mathbf{b}^L(\tau) + \mathbf{p}_0^L(\tau)\partial_\tau\theta(\tau) = \mathcal{L}^L(\tau)\mathbf{b}^L(\tau) + \sqrt{\kappa'}\mathbf{n}^L(\tau), \\
&\text{where } \mathcal{L}^L = \begin{pmatrix} \mathcal{L}_0^1 & \mathcal{T}^1 & & & \mathcal{T}^1 \\ \mathcal{T}^1 & \mathcal{L}_1^1 & \mathcal{T}^1 & & \\ & & \ddots & & \\ \mathcal{T}^1 & & & \mathcal{T}^1 & \mathcal{L}_{L-1}^1 \end{pmatrix}, \\
&\mathcal{L}_j^1(\tau) = -\begin{pmatrix} 1 & \bar{\beta}_j^2(\tau) \\ \bar{\beta}_j^{*2}(\tau) & 1 \end{pmatrix}, \text{and } \mathcal{T}^1 = \begin{pmatrix} ig & 0 \\ 0 & -ig \end{pmatrix}
\end{aligned}
\tag{5–4}
$$

Note that here the $\bar{\beta}_j$ are classical solutions given by (5–3) with some choice of k, corresponding to the pattern whose stability we are studying.

Remove τ-dependence For each $\mathcal{L}_j^1$, we can remove τ by picture transformation $\mathcal{L}_j^1(\tau) = -\mathcal{U}_g^{1\dagger}(\tau)\mathcal{M}_j^1\mathcal{U}_g^1(\tau)$,

$$\text{where } \mathcal{M}_j^1 = \begin{pmatrix} 1 & e^{4\pi ijk/L} \\ e^{-4\pi ijk/L} & 1 \end{pmatrix},\ \mathcal{U}_g^1(\tau) = \begin{pmatrix} e^{-2ig_k\tau} & 0 \\ 0 & e^{2ig_k\tau} \end{pmatrix}. \tag{5–5}$$

On the basis of (5–5), we can get $\mathcal{L}^L(\tau) = -\mathcal{U}_g^{L\dagger}(\tau)\mathcal{M}^L\mathcal{U}_g^L(\tau)$,

$$\begin{aligned} \text{where } \mathcal{U}^L(\tau) &= \begin{pmatrix} \mathcal{U}_g^1(\tau) & & & \\ & \mathcal{U}_g^1(\tau) & & \\ & & \ddots & \\ & & & \mathcal{U}_g^1(\tau) \end{pmatrix} \\ \text{and } \mathcal{M}^L &= \begin{pmatrix} \mathcal{M}_0^1 & \mathcal{T}^1 & & \mathcal{T}^1 \\ \mathcal{T}^1 & \mathcal{M}_1^1 & \mathcal{T}^1 & \\ & & \ddots & \\ \mathcal{T}^1 & & \mathcal{T}^1 & \mathcal{M}_{L-1}^1 \end{pmatrix}. \end{aligned} \tag{5–6}$$

We take the derivative of $\mathcal{U}^L\mathbf{b}^L$ and find the new motion function:

$$\begin{aligned} &\partial_\tau\left(\mathcal{U}^L\mathbf{b}^L\right) = \partial_\tau\mathcal{U}^L\mathbf{b}^L + \mathcal{U}^L\partial_\tau\mathbf{b}^L = \left(-2ig_k\mathcal{Z}^L - \mathcal{M}^L\right)\mathcal{U}^L\mathbf{b}^L, \\ &\text{where } \mathcal{Z}^L = \begin{pmatrix} 1 & & & \\ & -1 & & \\ & & \ddots & \\ & & & -1 \end{pmatrix} \text{ is } (2L \times 2L) \end{aligned} \tag{5–7}$$

Define $\mathbf{x} = \mathcal{U}^L(\tau)\mathbf{b}^L$ and it observes the motion function $\partial_\tau\mathbf{x} = \mathcal{S}^L\mathbf{x}$

$$\begin{aligned} \text{where } \mathcal{S}^L &= \begin{pmatrix} \mathcal{S}_0^1 & \mathcal{T}^1 & & \mathcal{T}^1 \\ \mathcal{T}^1 & \mathcal{S}_1^1 & \mathcal{T}^1 & \\ & & \ddots & \\ \mathcal{T}^1 & & \mathcal{T}^1 & \mathcal{S}_{L-1}^1 \end{pmatrix}, \\ \text{and } \mathcal{S}_j^1 &= \begin{pmatrix} -1-2ig_k & -e^{4\pi ijk/L} \\ -e^{-4\pi ijk/L} & -1-2ig_k \end{pmatrix} \end{aligned} \tag{5–8}$$

Having now a time-independent linear problem characterized by the linear stability matrix $\mathcal{S}^L$, we can proceed to study the stability of the patterns with different k.

Diagonalization With Fourier transformation $\mathcal{F}$, we are able to diagonalize $\mathcal{S}^L$. The transformation has another form $f_q = \frac{1}{\sqrt{L}}\sum_{j=0}^{L-1} e^{-2\pi ijq/L}x_j$ and its inverse reads $x_j = \frac{1}{\sqrt{L}}\sum_{q=0}^{L-1} e^{2\pi ijq/L}f_q$.

The Fourier transformation between f_q^+ and x_j^+ is similar but a complex conjugate of prior one. Using the dynamic equation for x_j, we can obtain the equation for f_q:

$$\begin{aligned}
\partial_\tau x_j &= (-1-2ig_k)x_j - e^{4\pi ijk/L}x_j^+ + ig(x_{j+1}+x_{j-1}) \\
\Rightarrow \partial_\tau f_q &= (-1-2ig_k)f_q - \frac{1}{\sqrt{L}}\sum_{j=1}^{L} e^{2\pi ijq/L}e^{4\pi ijk/L}x_j^+ \\
&\quad + \frac{ig}{\sqrt{L}}\left(\sum_{j=1} Le^{-2\pi ijq/L}x_{j-1} + \sum_{j=1} Le^{-2\pi ijq/L}x_{j+1}\right) \\
&= -1-2ig_k'(q)f_q - f_{q+2k}^+
\end{aligned} \tag{5–9}$$

where $g_k'(q) = g\left[\cos(2\pi k/L) - \cos(2\pi q/L)\right]$. We also derive the equation for f_{q+2k}^+, and find it connects with f_q. So the motion equation in Fourier space appear in pairs:

$$\begin{aligned}
&\partial_\tau \begin{pmatrix} f_q \\ f_{q+2k}^+ \end{pmatrix} = \mathcal{G}_q^1 \begin{pmatrix} f_q \\ f_{q+2k}^+ \end{pmatrix} \\
&\text{where } \mathcal{G}_q^1 = \begin{pmatrix} -1-2ig_k'(q) & -1 \\ -1 & -1+2ig_k'(q) \end{pmatrix}
\end{aligned} \tag{5–10}$$

Hereto we successfully diagonalize the matrix and decouple the system by rearranging the f_q by $\mathbf{f}_k = \left(f_1, f_{1+2k}^+, \cdots, f_L, f_{L+2k}^+\right)$:

$$\partial_t \mathbf{f}_k = \begin{pmatrix} \mathcal{G}_0^1 & & & \\ & \mathcal{G}_1^1 & & \\ & & \ddots & \\ & & & \mathcal{G}_{L-1}^1 \end{pmatrix} \tag{5–11}$$

Stability We calculate the eigenvalues of $\mathcal{G}_q^1$:

$$\lambda_\pm = -1 - i[g_k'(q) - g_k'(q+2k)] \pm \sqrt{1-[g_k'(q)+g_k'(q+2k)]^2}, \tag{5–12}$$

All have negative real parts, except when $q = k$, for which $\lambda = 0$. This means that all the pattern $\bar{\beta}_j(\tau)$ with a given k is stable against perturbations f_q with quasi-momentum $q \neq k$. On the other hands, the zero eigenvalue associated to perturbations $f_{q=k}$ is related to the invariance of the system under global phase transformations $\beta_j \to \beta_j e^{i\sigma}$, and is an example of Goldstone's theorem. Hence we proved that all of these patterns with different k are stable solutions.

For general Van der Pol lattices, we can still see patterns in the classical solutions. We show a simple example in Section A and show that these states are not always stable any more.

5.3 Analytical prediction for phase diffusion

With classical solutions we get in the last section, we are able to linearize the system. Like what we do for a single Van der Pol oscillator in Section 4.4.2, we calculate the variance growth for the coupled ones. For a system exhibit stable property of time crystal, the increase rate of variance should decrease by number of oscillators. With our linearization method, we have analytically

proved that it should be true for one-dimensional lattice. However, through numerical simulations of the exact stochastic equations, we show later that, still, this might not be enough for time-crystalline behavior.

Subsystem First, classically, ring of $L = L_0$ and $l = l_0$ is the same with a shorter ring of $L' = l_0$ and $l' = l_0$. It is obvious from the solution (5–3), because ring of L_0 oscillators repeats the same classical solution as a ring of length l_0. Here we give another intuition of this claim. $\beta_x, \beta_{x+1}, \cdots, \beta_{x+l_0-1}$ are l_0 consecutive oscillators in the longer Van der Pol ring. The last one, β_{x+l_0-1}, is coupled with β_{x+l_0}, which has the same phase as β_x. So the consecutive part is effectively a closed ring itself, or in other words, ring of $L' = l_0$ is a subsystem of ring of $L = L_0$.

Then we linearize the subsystem of $L' = l_0$, and obtain the linear stability matrix $\mathcal{L}^{l_0}$. It can be split to a more convenient form for the next derivation: $\mathcal{L}^{l_0} = \mathcal{L}_s^{l_0} + \mathcal{T}_s^{l_0} + \mathcal{T}_s^{l_0 T}$, where

$$\mathcal{L}_s^{l_0} = \begin{pmatrix} \mathcal{L}_0^1 & \mathcal{T}^1 & & & \\ \mathcal{T}^1 & \mathcal{L}_1^1 & \mathcal{T}^1 & & \\ & \ddots & \ddots & \ddots & \\ & & & \mathcal{T}^1 & \mathcal{L}_{l_0-1}^1 \end{pmatrix}, \quad \mathcal{T}_s^{l_0} = \begin{pmatrix} 0 & & & \\ & 0 & & \\ & & \ddots & \\ \mathcal{T}^1 & & & 0 \end{pmatrix} \tag{5–13}$$

Here superscript "T" means transpose operation.

We denote by $\mathbf{q}_0^{l_0\dagger}(\tau)$ (or $\mathbf{p}_0^{l_0}(\tau)$) the left (or right) Floquet eigenvector of $\mathcal{L}^{l_0}$ with zero eigenvalue. They satisfy

$$\begin{aligned} \dot{\mathbf{p}}_0^{l_0}(\tau) &= \mathcal{L}^{l_0}(\tau)\mathbf{p}_j^{l_0}(\tau), \\ \dot{\mathbf{q}}_0^{l_0\dagger}(\tau) &= -\mathbf{q}_j^{l_0\dagger}(\tau)\mathcal{L}^{l_0}(\tau). \end{aligned} \tag{5–14}$$

and normalization condition

$$\mathbf{q}_0^{l_0\dagger}(\tau)\mathbf{p}_0^{l_0}(\tau) = 1 \tag{5–15}$$

The whole system Using the representation above, we can linearize the system with $L = L_0$ easily, because there is periodicity in oscillators and $\mathcal{L}_{l_0+j}^1 = \mathcal{L}_j^1$. Its stability matrix reads

$$\mathcal{L}^{L_0} = \begin{pmatrix} \mathcal{L}_s^{l_0} & \mathcal{T}_s^{l_0} & & & \mathcal{T}_s^{l_0 T} \\ \mathcal{T}_s^{l_0 T} & \mathcal{L}_s^{l_0} & \mathcal{T}_s^{l_0} & & \\ & \ddots & \ddots & \ddots & \\ & & & \mathcal{T}_s^{l_0 T} & \mathcal{L}_s^{l_0} \end{pmatrix}. \tag{5–16}$$

The final equation for integrating variance is also similar:

$$V^{L_0}(\tau) = \overline{[\theta(\tau) - \theta(0)]^2} = \gamma \int_0^\tau d\tau' \mathbf{q}_0^{L_0\dagger}(\tau') \mathcal{N}^{L_0}(\tau') \mathbf{q}_0^{L_0 *}(\tau'), \tag{5–17}$$

Here $\mathcal{N}^{L_0}$ is the correlation matrix:

$$\begin{aligned}\mathcal{N}^{L_0} &= \begin{pmatrix} \mathcal{N}^{l_0} & & & \\ & \mathcal{N}^{l_0} & & \\ & & \ddots & \\ & & & \mathcal{N}^{l_0} \end{pmatrix}, \\ \text{where } \mathcal{N}^{l_0} &= \begin{pmatrix} \mathcal{N}_0^1 & & & \\ & \mathcal{N}_1^1 & & \\ & & \ddots & \\ & & & \mathcal{N}_{l_0-1}^1 \end{pmatrix} \\ \text{and } \mathcal{N}_j^1 &= \begin{pmatrix} -\bar{\beta}_j^2(\tau) & 2 \\ 2 & -\bar{\beta}_j^{*2}(\tau) \end{pmatrix}\end{aligned} \tag{5–18}$$

With the knowledge of the subsystem, we claim the Floquet eigenvector $\mathbf{p}_0^{L_0}(\tau)$ is a simple repetition of $\mathbf{p}_0^{l_0}(\tau)$ with a normalization factor χ_p, namely, $\mathbf{p}_0^{L_0} = \chi_p \left(\mathbf{p}_0^{l_0 T}, \mathbf{p}_0^{l_0 T}, \cdots\right)^T = \chi_p \partial_\tau \bar{\boldsymbol{\beta}}$, because

$$\mathcal{L}^{L_0}\mathbf{p}_0^{L_0} = \chi_p \begin{pmatrix} (\mathcal{L}_s^{l_0} + \mathcal{T}_s^{l_0} + \mathcal{T}_s^{l_0 T})\mathbf{p}_0^{l_0} \\ \vdots \\ (\mathcal{L}_s^{l_0} + \mathcal{T}_s^{l_0} + \mathcal{T}_s^{l_0 T})\mathbf{p}_0^{l_0} \end{pmatrix} = \chi_p \begin{pmatrix} \partial_\tau \mathbf{p}_0^{l_0} \\ \vdots \\ \partial_\tau \mathbf{p}_0^{l_0} \end{pmatrix} = \partial_\tau \mathbf{p}_0^{L_0}. \tag{5–19}$$

In the linearized equation (5–4), $\mathbf{p}_0^{L_0}(\tau)$ is defined directly as $\partial_\tau \bar{\boldsymbol{\beta}}$, so the norm χ_p is fixed to 1. On the other hands, we also have $\mathbf{q}_0^{L_0\dagger}(\tau) = \chi_q \left(\mathbf{q}_0^{l_0\dagger}, \mathbf{q}_0^{l_0\dagger}, \cdots\right)$. Its norm factor χ_q is determined by Eq. (5–15):

$$\begin{aligned} \mathbf{q}_0^{L_0\dagger}\mathbf{p}_0^{L_0} &= \frac{L_0}{l_0}\chi_q \mathbf{q}_0^{l_0\dagger}\mathbf{p}_0^{l_0} = 1, \\ \Rightarrow \chi_q &= \frac{l_0}{L_0} \end{aligned} \tag{5–20}$$

In a word, the Floquet eigenvectors for the system are:

$$\begin{aligned} \mathbf{p}_0^{L_0} &= (\mathbf{p}_0^{l_0 T}, \cdots, \mathbf{p}_0^{l_0 T})^T \\ \mathbf{q}_0^{L_0\dagger} &= \frac{l_0}{L_0}(\mathbf{q}_0^{l_0\dagger}, \cdots, \mathbf{q}_0^{l_0\dagger}) \end{aligned} \tag{5–21}$$

Plug (5–21) into (5–17), we get

$$V^{L_0}(\tau) = \frac{l_0}{L_0} V^{l_0}(\tau), \tag{5–22}$$

which is our final analytical result. Since pattern l_0 and subsystem's variance is fixed, we predict the system's variance V^{L_0} is inverse proportional to the system's size L_0. If it is true, the macroscopical coupled Van der Pol system is a time crystal when properly initialized. When the system has a large number of oscillators (for example, Avogadro's number), the variance will be kept low for almost infinite time.

5.4 Stochastic simulation and time-crystalline order

In Section 4.4.2, we show the stochastic simulation for a single Van der Pol oscillator and verify the linear variance growth. In this section, we apply the same technique to the coupled Van der Pol

systems and plot the variance growth of them. $l = 1$ case is chosen and all oscillators are initialized to be synchronized. Besides 1D Van der Pol rings, we also simulate the 2D, 3D and all-to-all coupled (A2A) Van der Pol lattices, which we haven't analytically researched. Oscillators in a 2D system are coupled with their four neighbors (up, down, left, right), and ones in a 3D system are coupled with six neighbors. In an A2A coupled system, each oscillator is coupled to everyone else.

5.4.1 Slope of variance growth

In the numerical simulation, (5–2) is simulated for 32000 times for each parameter combination, which consists of different connectivity and different L. For every stochastic trajectory, we calculate the phase $\theta_j(\tau)$ for all modes β_j, by $\theta_j(\tau) = \mathrm{Im}\left[\ln(\beta_j(\tau)/\bar{\beta}_j(\tau))\right]$. Then the variance $V_j(\tau)$ of $\theta_j(\tau)$ is obtained. In one sub-figure of Figure 5–2, $V_j\tau$ is plotted with different colors.

In the numerical simulation, these coupled systems' variances display a similar trend versus τ. we exhibit the variance growth with different L_0 and lattice dimension, where $g = 1$ and $\kappa' = 10^{-6}$. $V(\tau)$ is divided by $s_0 = \frac{3}{2}\kappa'$ in the plot, which was the slope of $V^1(\tau)$ for a single oscillator.

After carefully studying, comparing and fitting these curves, we come up with these conclusions. All of the curves with different sizes have the same beginning, whose slope is exactly 1. It is also true for 1D, 2D, 3D and A2A case. This initial variance increase violates our prediction through linearization. Such an abnormal effect may come from our initial assumption in (5–4), which claims all modes are strongly coupled and share the same variable θ. The violation indicate that, the coupling cannot synchronize the oscillators instantaneously, but requires some time to reach the state in which all phases are locked to the global θ. Onece in this stage, variance increases with slope s_0/L according to our theory.

In a word, there are two stages of variance growth: first, the variances grow with slope s_0, and then the slopes decrease to s_0/L_0. Figure 5–3a shows the relationship between second stage's slope and size of lattice. The slope of the lattice is acquired by $s = dV/d\tau$, and in the figure, we plot $\lg(s/s_0)$ versus $\lg(L)$. The figure also includes a reference line $y = -x$. All dots are on the line, indicating that $s = s_0/L$.

5.4.2 Candidate for time crystal

Our goal is realizing a system with low phase diffusion in a long time. In our model, macroscopical coupled Van der Pol lattices do have the potential to achieving a stable variance, because with enormously large L like Avogadro's number, the second stage's slope goes to zero. Different from our analytical result, it doesn't mean the system becomes robust against quantum fluctuation, because of the variance growth at first stage. To research it, we fit the second stages of variance growth with line $V(\tau) = s\tau + V_0$, and V_0 is a initial bias for the linear growth. Figure 5–3b plots the relationship between $\lg(V_0)$ and $\lg(L)$.

From the figure, it's clear that except A2A systems, systems with finite connectivity have a V_0 proportional to L^r, where r is a positive number. Although r is reduced as lattices' dimension increase, we believe it always keeps positive, which makes the variance explode in a macroscopical system and destroys the time-crystalline order. Variance suppression can only be achieved in A2A system, when connectivity and L reach infinity at the same time. In Figure 5–3b, we observe a

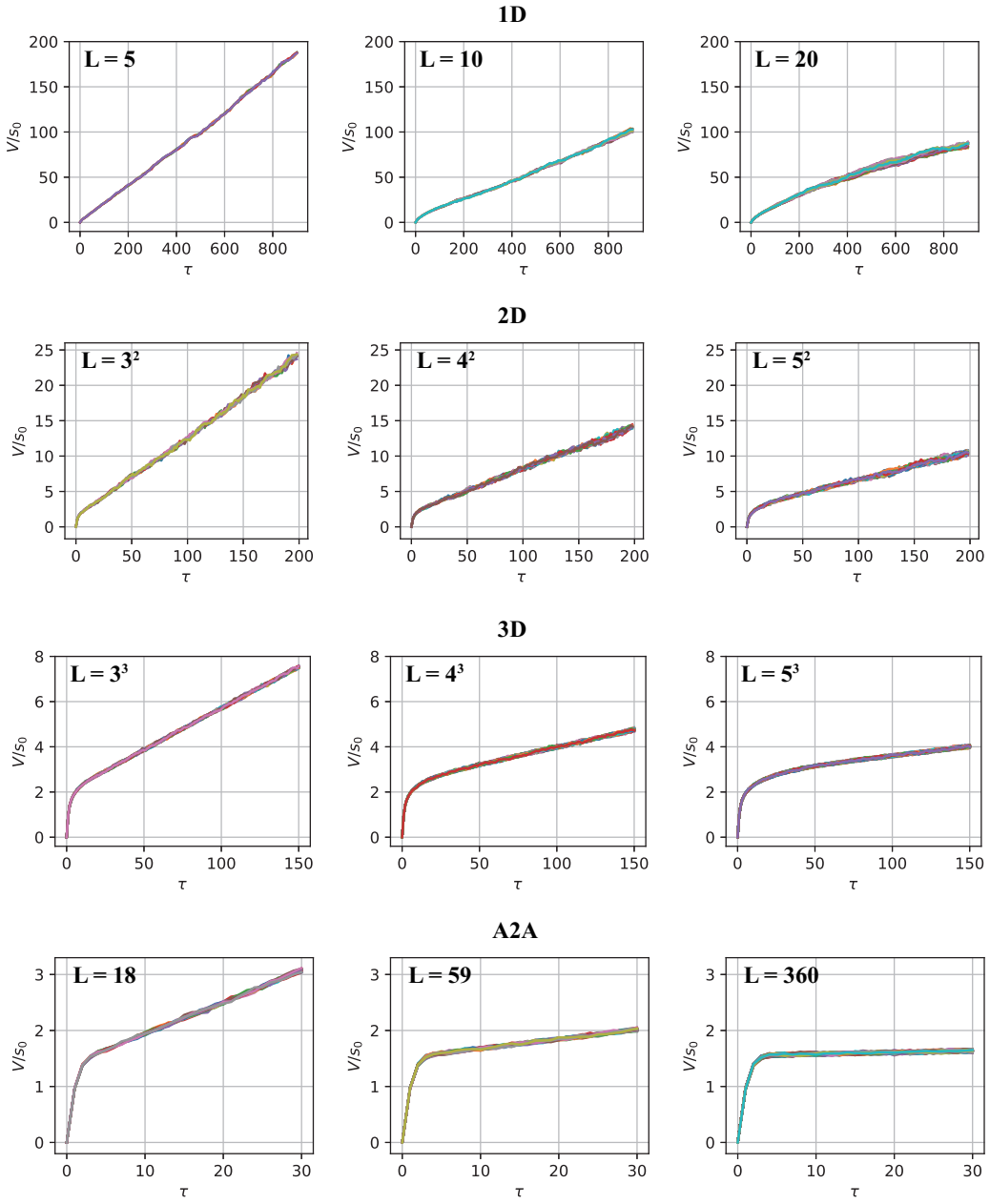

Figure 5–2 Variance growth

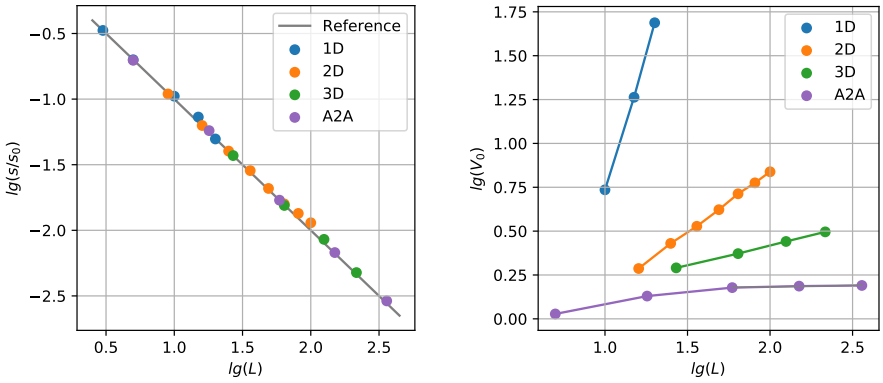

a) Variance growth slope versus the size of lattice lg(L). The gray line is plotted by function $y = -x$.

b) Variance growth bias versus the size of lattice lg(L).

Figure 5–3 Linear fit for the variance growth

gradually saturating V_0 in A2A system when L becomes larger. It means that only in an all-to-all coupled system, the phase variance is kept low against quantum fluctuations. Hereto we finally prove that the time-crystalline order can be achieved in a macroscopical all-to-all coupled Van der Pol lattice.

Our theory is also consistent with the reality that we haven't seen this kind of time-crystal in nature or in an experiment, because the time-crystalline order is hard to achieve according to (5–22). First, there are too many of classically stable patterns in a macroscopical system, and with natural (random) initialization, a lattice is more likely to fall onto a state without repeated patterns, which is important to keep l_0/L_0 small. Second, a macroscopical all-to-all coupled system is hard to achieve with existing platforms.

Chapter 6 Conclusion

In this thesis, we give a proof of the existence of self-sustained quantum oscillation and show an architecture of it with coupled Van der Pol lattice, with which we achieve time crystalline order in an open system.

In Chapter 3, we introduce the ATS system, a novel kind of superconducting circuits whose Hamiltonian have a third order coupling term. We generalize it to a four mode system and adjust the circuit parameters to achieve down-conversion. Using effective theory, we eliminate the irrelevant fields and finally get a single-mode systems. In the master equation, the system has a characteristic pumping term and a non-linear damping term, indicating it is effectively a quantum Van der Pol oscillator.

In Chapter 4, a single Van der Pol oscillator is studied classically and quantum mechanically. By plotting the phase diagram of the Van der Pol oscillator in classical limit, we find it evolve in limit cycle under certain conditions. In the limit cycle phase, classical oscillator runs in a closed phase-space trajectory and keeps oscillating forever. However, we show a quantum Van der Pol oscillator will soon leave such an oscillatory behavior, which is far from equilibrium, and is vulnerable to quantum fluctuations. To prove it, we define phase variance as a measure of maintenance of time-crystalline order, which is kept if variance small in infinite long time. With linearization and Floquet method, we find the variance grows linearly in time, and it is also verified by a numerical simulation. Hence, a single Van der Pol oscillator can not display time-crystalline order.

With the knowledge of coupled Van der Pol oscillators are synchronized, we focus on building time crystal with the coupled Van der Pol lattices in Chapter 5. A non-driven 1D Van der Pol lattice has a set of limit cycle solutions, all of which are stable classically. Some solutions have spacial patterns that repeat along the 1D Van der Pol ring. Adapting a simple matrix analysis method, we analytically find that the coupling effect suppresses the variance growth inverse proportional to the lattice size. In the numerical simulation, we observe an unpredicted initial variance growth stage besides the variance growth suppression, which results in a initial variance bias. For 1D, 2D and 3D lattices, such initial variance biases scale with a positive power of the lattice size, which means that by the time the quantum fluctuations are suppressed, the time-crystalline order is already lost. But for the all-to-all coupled model, its initial variance is a constant and independent of the system size. As a result, time crystalline order is achieved in a finite time for a large all-to-all coupled system.

In a word, what we achieve is building a self-sustained quantum oscillators and breaking time translation symmetry with an open system. Besides superfluid, whose oscillation is sustained by particle number conservation, and Floquet time crystal, which only breaks the discrete time translation symmetry, our work gives a novel realization of breaking continuous time translation symmetry and achieving time-crystalline order in open systems.

Appendix A Patterns in a general Van der Pol ring

Classically, we proved that a synchronized state is always stable in a 1D non-driven Van der Pol ring in Section 5.2, but it's not true in every general Van der Pol lattices. We here choose a system with $L = 12$, $\Delta^2 = 0.3$ and $F^2 = 0.2$ as an example.

For a Van der Pol ring, there exist various spacial patterns, and similar phases patterns repeat on the ring periodically. Some common patterns of the non-driven systems are shown in Eq. (5–3) and Figure 5–1 shows and we prove that they are all stable states. Here we give another state, who has phase $(0, 0, \pi, \pi, 0, 0, \pi, \cdots)$, named by us as a pattern of $l = 2 \times 2$. This state is unexpectedly stable among a wild range of parameters.

We analyze the linear stability matrix $\mathcal{L}$ of these state with different coupling g, which controls the stability of the system. The largest eigenvalue of $\mathcal{L}$ is plotted in Figure A–1.

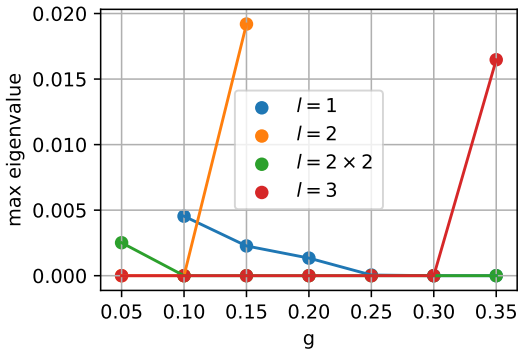

Figure A–1 Max eigenvalue of $\mathcal{L}$

A linear stability matrix with eigenvalues larger than 0 means the system is not stable and will leave the current state spontaneously, let along there is quantum fluctuations. Indicated by Figure A–1, the system is unstable under some situations. For state with certain pattern, we predict that there is a phase transition when changing g. And Section B.2 will focus on finding the transition.

Appendix B Synchronization of Van der Pol lattice in classical limit

According to[9], both quantum and classical Van der Pol oscillators have synchronization effect, which makes every oscillator's phase locked. In this appendix, we are going to analyze the synchronization effect of our Van der Pol model, which may give our some inspirations about the architecture of time crystal.

L coupled Van der Pol oscillators are described by a master equation:

$$\begin{aligned}\partial_t\hat{\rho} =& -i\left[\hat{H},\hat{\rho}\right]+\sum_{j=0}^{L-1}\left(D_{a_j}\left[\hat{\rho}\right]+\frac{\kappa'}{2}D_{a_j^2}\left[\hat{\rho}\right]\right)\\ \hat{H} =& \sum_{j=0}^{L-1}\left[-\Delta\hat{a}_j^\dagger\hat{a}_j+\left(-i\frac{F}{\sqrt{\kappa'}}\hat{a}_j^\dagger+H.c.\right)-g_c\left(\hat{a}_j^\dagger\hat{a}_{j+1}+\hat{a}_{j+1}^\dagger\hat{a}_j\right)\right]\end{aligned} \tag{B–1}$$

Classically, the system is described by a stochastic Langevin equation. In the equation, $\boldsymbol{\beta}=\sqrt{\kappa'}(\alpha_0,\alpha_1,\cdots,\alpha_{L-1})^T$. For simplicity, we add a complex noise $\boldsymbol{\eta}(\tau)$ to the equation.

$$\begin{aligned}\partial_\tau\boldsymbol{\beta} =& \mathbf{A}(\boldsymbol{\beta})+\mathcal{B}\boldsymbol{\eta}(\tau)\\ \mathbf{A}(\boldsymbol{\beta}) =& \begin{pmatrix} & \cdots & \\ F+\beta_j\left(i\Delta+1-\left|\beta_j\right|^2\right)+ig\left(\beta_{j-1}+\beta_{j+1}\right) & & \\ & \cdots & \end{pmatrix}\\ \mathcal{B} =& \begin{pmatrix}\gamma_c & & \\ & \cdots & \\ & & \gamma_c\end{pmatrix}\end{aligned} \tag{B–2}$$

$\gamma_c\neq 0$ will introduce noises to the system, while $g_c\neq 0$ will synchronize the oscillators. If all β_j is at the same phase, they will evolve with limit cycles with an effective detuning $\Delta+2g_c$. Specifying Δ, F and g_c4 determines the limit cycle.

B.1 Observables

To exhibit coupled Van der Pol oscillators are synchronized against noise, we selected two observables: the average of β_j over oscillators and the diffusion of phase.

First observable: $\left|\bar{\beta}\right|=\frac{1}{L}\left|\sum_j\beta_j\right|$. Large average means they are in the synchronized phase and small means they are with random phase.

Second observable: Variance of θ_j. In phase space, we define the phase of each oscillator by setting a oscillating reference point $\beta_{ref}(\tau)$ on the limit cycle. Since each oscillator β_j evolves periodically on the limit cycle, we can always find a time θ_j that $\beta_j(\tau)=\beta_{ref}(\tau+\theta_j)$. To achieve this, we first find the period T of the limit cycle. Then we project the points (β_j in phase space) to the effective limit cycle. With a initial β_{ref} point, we find the corresponding phase θ_j ($0<\theta_j<T$). Then we analyze the variance and the average of the θ_j.

B.2 Results

We check the synchronization effect with different parameters.

B.2.1 Disturbance and synchronization

When $\Delta^2 = 0.3$ and $F^2 = 0.2$, the system evolve in a limit cycle. The original system, noisy system and the coupled noisy system are compared in Figure B–1. In the figure, we compare a noisy system, a coupled noisy system and a reference, noiseless effective system. The noisy system has $\gamma_c = 0.1$ (orange line), and when turning on coupling, $g_c = 0.16$ (green line). The noiseless effective system has $g_c = 0$ and $\gamma_c = 0$ (blue line). And there is 10 oscillators coupled together ($L = 10$) and initialized to be synchronized ($l = 1$). In the figure, three sub-figures are plotted, which are about two observables ($\left|\bar{\beta}\right|$ on the upper left, and var(θ_j) on the lower left) and phase space trajectories (right). Clearly, $|\beta|$ of noisy oscillators converge to the average, and its variance of θ_j goes to saturation, too. In contrast, coupled oscillator keeps in phase and remain same with the effective one. Moises make oscillator de-phasing while coupled oscillators stay synchronized.

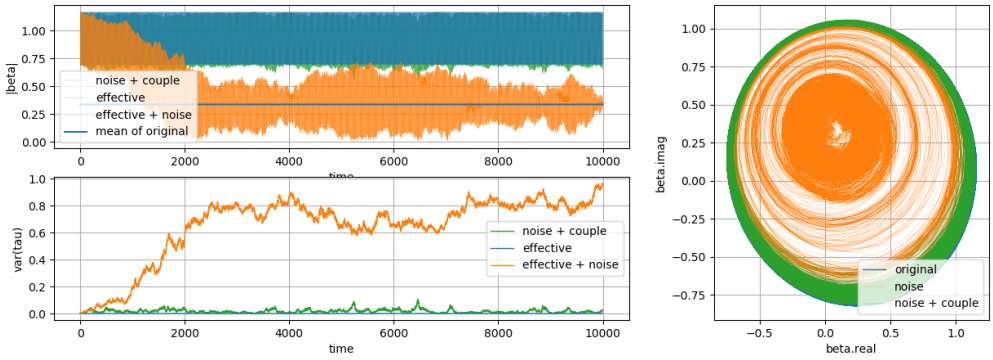

Figure B–1 Disturbance and synchronization.

I also display each of the β_j in phase space in Figure B–2. Dots with the same color means they are different oscillators on the ring at the same time, we displays oscillators at 7 different times. At the same time, coupled oscillators have similar phases, and noisy ones distribute randomly. Also, we find all dots evolve along the effective limit cycle (grey line).

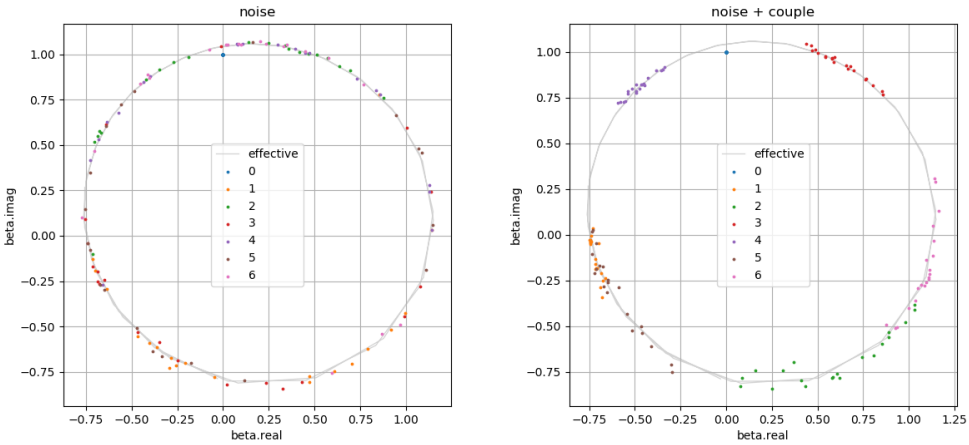

a) Noisy oscillators b) Coupled oscillators

Figure B–2 Classical phase distribution

B.2.2 Phase transition

Coupling coefficient g_c have a strong effect on synchronization, because it directly controls whether the state is steady. With previous parameter setting, $g_c \approx 0.12$ is the critical point. When $g_c > 0.12$, β_j starts to synchronize with each other and will not be disturbed by the noise. We show a typical result in Figure B–3. We simulate the coupled system at $g = 0.1$, $g = 0.13$ and $g = 0.16$, all starting from a $l = 1$ synchronized state.

Here we clearly observe a phase transition from Figure B–3a to Figure B–3b. When g is smaller than the critical point, the system is unstable and easily effected by noise, vise versa. Somrthing very interesting is that, the system with low g doesn't just simply become noisy, but fall on another patterns of synchronized state. In Figure B–3a, the final pattern it reaches is state with $l = 2$.

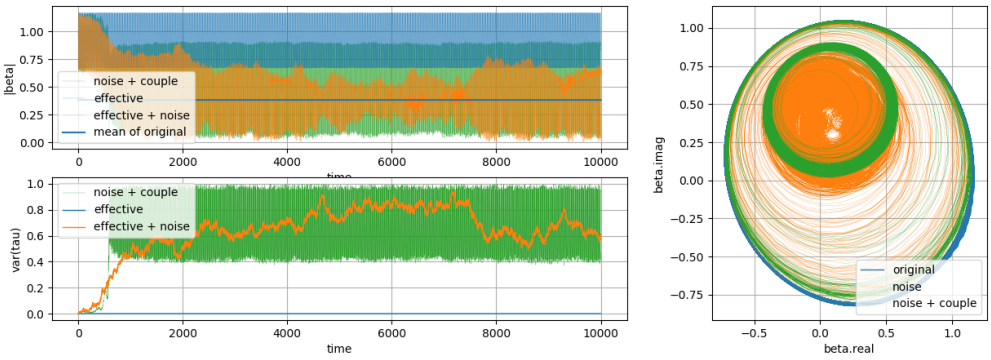

a) $\gamma_c = 0.1$, $g_c = 0.1$.

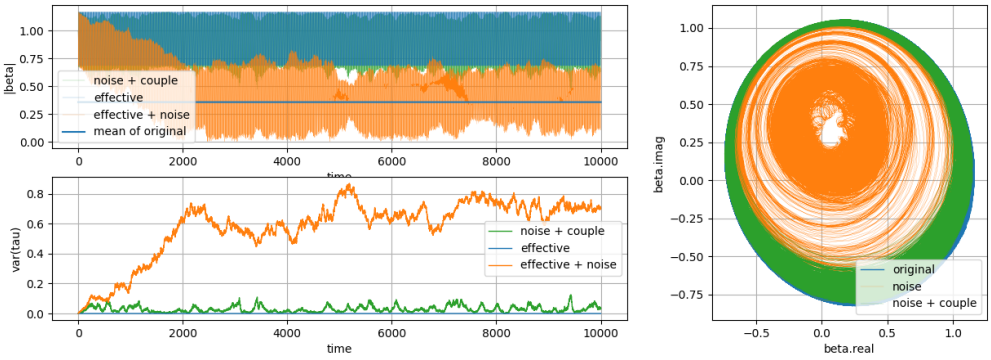

b) $\gamma_c = 0.1$, $g_c = 0.13$.

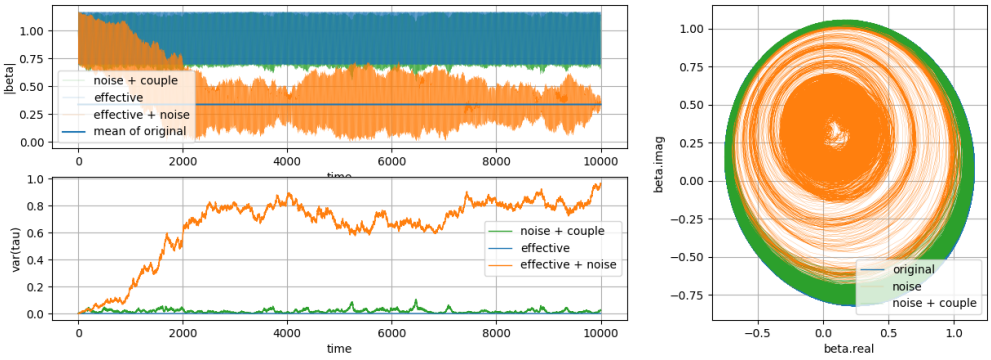

c) $\gamma_c = 0.1$, $g_c = 0.16$.

Figure B–3 Varying coupling coefficient ($L = 10$)

B.2.3 Changing number of oscillators

As Figure B–4 shows, increasing L from 10 to 100 makes the system more unstable, which result from the increase of the critical point. When $L = 100$, the critical point of g_c increases to about 0.13.

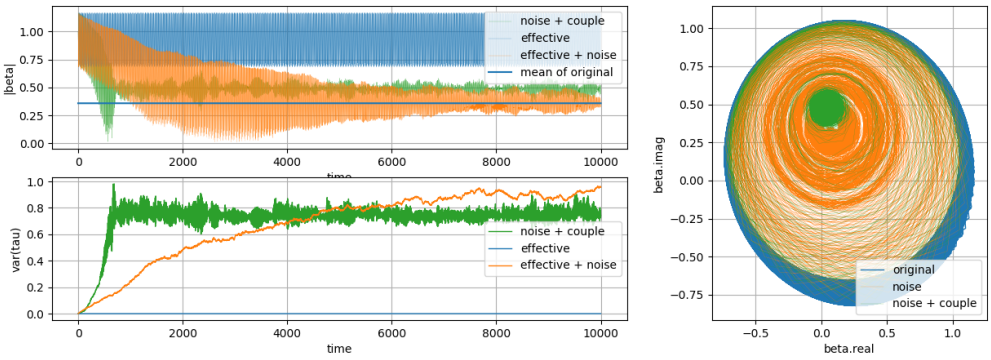

a) $\gamma_c = 0.1$, $g_c = 0.13$.

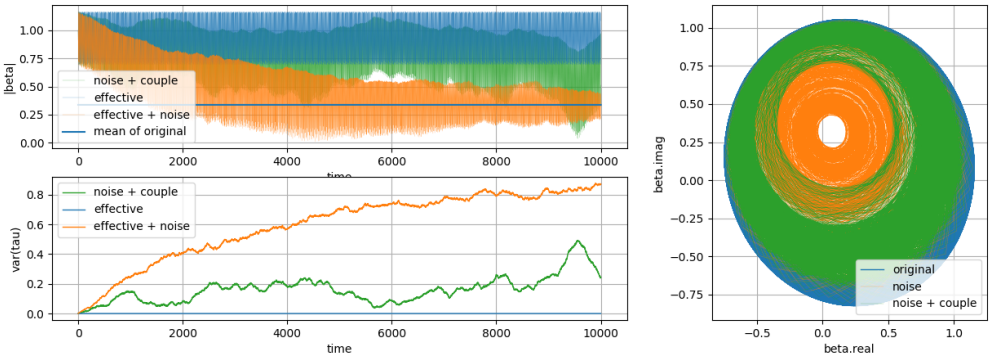

b) $\gamma_c = 0.1$, $g_c = 0.16$.

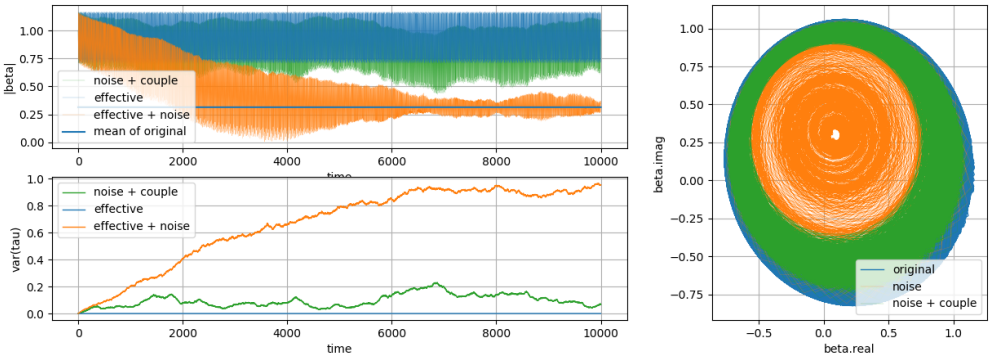

c) $\gamma_c = 0.1$, $g_c = 0.20$.

Figure B–4 Longer array of oscillators ($L = 100$)

This phase diffusion can also be visualized with scattering oscillators on the phase space in Figure B–5. Compared with Figure B–2, dots are more dispersed with larger L.

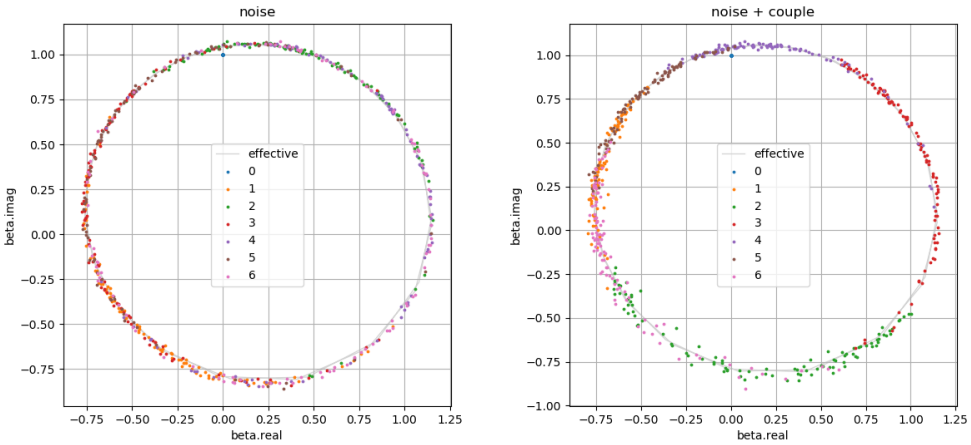

a) Noisy oscillators b) Coupled oscillators

Figure B–5 Dots with different colors represent β_j at different time. ($L = 100$)

Besides, we visualize the phase fluctuation $\left(\theta_j - \frac{1}{L}\sum_j \theta_j\right)/T$ of each oscillators versus time in Figure B–6. $\tau = 0 \sim 50$ and $\tau = 2000 \sim 2050$ are plotted in the figure. At the beginning, oscillators are pulled by the noise and gradually depart from the average. After $\tau = 2000$, these oscillators evolve into a stable pattern, which has relative large fluctuation. This is because the oscillators are only coupled with neighbors. Small differences will accumulate when the array becomes longer. I believe, simply increasing L may even harm the global synchronization for classical Van der Pol oscillators. At least, we should introduce some remote connections.

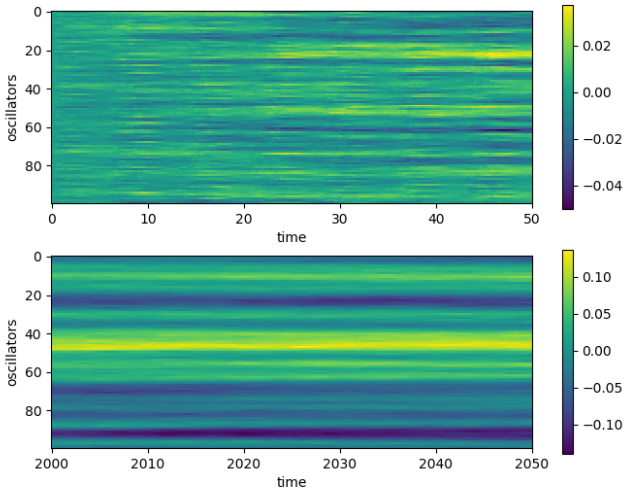

Figure B–6 Classical phase diffusion

Bibliography

[1] Wilczek F. Quantum time crystals[J]. Physical review letters, 2012, 109(16): 160401.

[2] Shapere A, Wilczek F. Classical time crystals[J]. Physical review letters, 2012, 109(16): 160402.

[3] Watanabe H, Oshikawa M. Absence of quantum time crystals[J]. Physical review letters, 2015, 114(25): 251603.

[4] Prokof’ ev N V, Svistunov B V. Algebraic time crystallization in a two-dimensional superfluid[J]. Journal of Experimental and Theoretical Physics, 2018, 127(5): 860-864.

[5] Khemani V, Moessner R, Sondhi S. A brief history of time crystals[J]. ArXiv preprint arXiv:1910.10745, 2019.

[6] Iemini F, Russomanno A, Keeling J, et al. Boundary time crystals[J]. Physical review letters, 2018, 121(3): 035301.

[7] Van der Pol B. A theory of the amplitude of free and forced triode vibrations, Radio Rev. 1 (1920) 701-710, 754-762[J]. Selected Scientific Papers, 1960, 1.

[8] Kanamaru T. Van der Pol oscillator[J]. Scholarpedia, 2007, 2(1): 2202.

[9] Lee T E, Sadeghpour H. Quantum synchronization of quantum van der Pol oscillators with trapped ions[J]. Physical review letters, 2013, 111(23): 234101.

[10] Navarrete-Benlloch C, Weiss T, Walter S, et al. General linearized theory of quantum fluctuations around arbitrary limit cycles[J]. Physical review letters, 2017, 119(13): 133601.

[11] Walter S, Nunnenkamp A, Bruder C. Quantum synchronization of a driven self-sustained oscillator[J]. Physical review letters, 2014, 112(9): 094102.

[12] Lörch N, Amitai E, Nunnenkamp A, et al. Genuine quantum signatures in synchronization of anharmonic self-oscillators[J]. Physical review letters, 2016, 117(7): 073601.

[13] Lee T E, Chan C K, Wang S. Entanglement tongue and quantum synchronization of disordered oscillators[J]. Physical Review E, 2014, 89(2): 022913.

[14] Davis-Tilley C, Teoh C, Armour A. Dynamics of many-body quantum synchronisation[J]. New Journal of Physics, 2018, 20(11): 113002.

[15] Lescanne R, Villiers M, Peronnin T, et al. Exponential suppression of bit-flips in a qubit encoded in an oscillator[J]. Nature Physics, 2020, 16(5): 509-513.

[16] Husimi K. Some formal properties of the density matrix[J]. Proceedings of the Physico-Mathematical Society of Japan. 3rd Series, 1940, 22(4): 264-314.

[17] Wigner E P. On the quantum correction for thermodynamic equilibrium[G]. in: Part I: Physical Chemistry. Part II: Solid State Physics. Springer, 1997: 110-120.

[18] Glauber R J. The quantum theory of optical coherence[J]. Physical Review, 1963, 130(6): 2529.

[19] Schaffter T. Numerical integration of SDEs: a short tutorial[R]. 2010.

[20] Floquet G. Sur les equations differentielles lineaires e coefficients périodiques[C]. in: Annales scientifiques de l'Ecole normale superieure: vol. 12. 1883: 47-88.

[21] Navarrete-Benlloch C. Open systems dynamics: Simulating master equations in the computer[J]. ArXiv preprint arXiv:1504.05266, 2015.

Acknowledgements

这篇毕业设计将成为我在本科期间最满意、最自豪的作品。我向它倾注了我对世界的理解与爱，尽管它们还远远不够成熟。对我来说，它不仅仅是一段科研的结语，而是我的意识在成长过程中产生的文字积淀，沉淀着我的世界观和梦想。然而，当我回看我的成长之路时，我发现它要比我意料中的坎坷很多，路上遍布艰险与抉择。帮助我昂首前进的，是无数双手，他们托举着我，走向这四年的终点。在此，我想感谢伴我走过四年人生路的所有人。

我感谢上海交通大学以及物理与天文学院，为我提供了专业却不失多元性的生活环境和学习资源，从校园设施、社团文化，到优秀课程、访学活动，都为我的成长提供了绝佳的平台。

感谢我的导师 Carlos Navarrete-Benlloch 教授塑造了我的物理梦想，向我展现了这个用数学语言描述的世界，通过亲自耐心地指导我的学习和科研，让我明白了科学探索的魅力。感谢 Carlos 在这个毕业设计中和我的每一次讨论，一直在为这个课题引导方向、制定目标，让我充满方向感与满足感。此外，我还要感谢 Carlos 作为我生活上的榜样，时刻提醒我要兼收并蓄，并且永不言弃。

感谢物理系、数学系、计算机系、建筑系等曾经教导过我的各位老师们，向我展示了这个世界浓缩的文明，一步步构筑起我的知识体系。何峰老师的量子力学课、张鹏杰教授的广义相对论课、许志钦老师的深度学习实践、Yale Patt 教授的计算机系统导论等，不仅是我知识框架的支柱，还将成为我永远的精神食粮。

感谢来自天文协会、物理学院、考拉格、高中等的朋友们，与我分享这个生活的美好，陪伴我一起探寻有趣的文化、科技和游戏。感谢张骞为我分享人生心得，沈丛带领我领略宇宙原理，戴暄耕陪伴我周游 MC 世界，以及所有朋友们对我的支持与陪伴。

最后，也是最重要的，我感谢父母对我多年如一日的爱与塑造，家是我永远的港湾。

四年悄然逝去，但是故事与情谊是永恒的，我将永远铭记。愿我的未来也如现在一样充满爱与激情。